Journal of Applied Analysis and Computation
Volume 16, Number 5, October 2026, 2639–2667
Website:http://www.jaac-online.com
DOI:10.11948/20250379

(QUANTUM, DEFORMED)-FRACTIONAL COMPLEX STEPS: THEORY, ENTROPY ANALYSIS, AND IMAGING APPLICATIONS

Rabha W. Ibrahim[1,2†] and Dumitru Baleanu[3,4]

Abstract We introduce a generalized quantum (q,τ)-fractional complex step framework for the numerical evaluation of fractional derivatives based on quantum-deformed special functions. We develop rigorous definitions of the (q,τ)-Fractional Complex Step Method (FCSM), establish convergence and error estimates under analytic regularity, and derive fractional entropy identities, including Tsallis and Shannon H-theorems, for generalized diffusion systems. Analytical properties of the (q,τ)-Gamma function and related operators are presented, together with illustrative numerical examples. The proposed framework extends classical complex step methods and provides a mathematically rigorous toolset for analyzing fractional operators in both pure and applied contexts.

Keywords Fractional complex step method, (q,τ)-Gamma function, environmental management, pollution transport modeling, fractional calculus, parameter calibration, sustainability assessment, memory effects.

MSC(2010) 26A33.

1. Introduction

Fractional calculus has emerged as a powerful mathematical tool for describing systems with memory, nonlocality, and hereditary properties that cannot be adequately captured by classical integer-order derivatives [8, 12, 33]. In recent years, special attention has been devoted to generalized fractional operators based on deformed special functions, which allow more flexible modeling of complex dynamical behaviors [25, 28, 29]. Among these, the (q,τ)-Gamma function plays a fundamental role as a deformation of the classical Gamma function, introducing the parameters q and τ as quantum-inspired regulators of scaling and memory effects. This generalization provides a unified framework for extending classical operators, enabling their application to systems that exhibit non-classical or anomalous dynamics [6, 11, 13].

Parallel to these developments, the *Complex Step Method* (CSM) has gained recognition as a stable and highly accurate technique for numerical differentiation [1, 23]. The essence of the method is to approximate derivatives by perturbing the input with an imaginary increment and extracting the imaginary component of the function evaluation [2, 15]. This approach avoids subtractive cancellation errors inherent in finite difference schemes, and when extended to frac-

†The corresponding author.
[1]Department of Mathematics, Saveetha School of Engineering, Saveetha Institute of Medical and Technical Sciences SIMATS, Chennai, Tamil Nadu 602105, India
[2]Information and Communication Technology Research Group, Scientific Research Center, Al-Ayen University, Thi-Qar, Nasiriyah 64001, Iraq
[3]Department of Computer Science and Mathematics, Lebanese American University, Beirut, Lebanon
[4]Institute of Space Sciences, R76900 Magurele-Bucharest, Romania
Email: rabhaibrahim@yahoo.com(R. W. Ibrahim), dumitru.baleanu@gmail.com(D. Baleanu)

tional orders, it leads to the *Fractional Complex Step Method* (FCSM). By incorporating the (q,τ)-Gamma function into this framework, we obtain the (q,τ)-FCSM, a novel scheme capable of capturing deformed fractional derivatives while retaining the numerical stability of the complex step. The Fractional Complex Step Method (FCSM) is a numerical differentiation technique that extends the classical complex step approach to fractional-order derivatives. Its principle lies in perturbing the argument of a function with an imaginary increment scaled by a fractional power, and then extracting the imaginary part of the evaluation to approximate the derivative. Unlike finite difference methods, which often suffer from catastrophic subtractive cancellation, the FCSM avoids round-off errors and provides stable results even for very small step sizes. When combined with the (q,τ)-Gamma function, the method is capable of accurately computing deformed fractional derivatives, bridging the gap between numerical stability and theoretical generalization [3, 16, 17, 26]. This makes the FCSM an effective tool for analyzing systems governed by fractional calculus in physics, engineering, and environmental modeling [18–20].

The applications of such a framework are wide-ranging. In physics, the (q,τ)-FCSM can be applied to anomalous diffusion processes, non-Hermitian quantum mechanics, and memory-dependent oscillators [5, 14]. In engineering, it provides robust techniques for control and stability analysis of fractional-order systems, particularly in systems with hereditary damping [4, 21]. In environmental science, where nonlocal effects and long-term memory are critical, the (q,τ)-FCSM offers new tools for modeling pollutant transport, ecological interactions, and sustainability scenarios [9, 24]. Furthermore, the symmetric version of the method improves numerical convergence and stability, making it a suitable candidate for real-world large-scale simulations [7, 10].

The (q,τ)-Fractional Complex Step Method (FCSM) provides several notable advantages when applied to environmental management models. First, the method offers high numerical stability, avoiding subtractive cancellation errors that commonly affect finite difference approximations, thereby ensuring accurate simulation of long-term environmental processes with memory effects. Second, the incorporation of the (q,τ)-Gamma function allows flexible adjustment of memory and scaling parameters, enabling the modeling of heterogeneous ecological systems, such as pollutant dispersion, groundwater flow, and climate-ecosystem interactions. Third, the symmetric formulation of the (q,τ)-FCSM enhances error cancellation, producing more reliable results even under small perturbations, which is critical in decision-making scenarios where small parameter changes can strongly influence sustainability outcomes. Finally, the method's ability to capture both local and nonlocal effects makes it a valuable tool for designing optimal environmental policies, supporting predictive modeling, and guiding adaptive strategies for sustainable resource management. Table 1 highlights the comparative advantages of the (q,τ)-Fractional Complex Step Method (FCSM) over classical finite differences and standard fractional schemes. Unlike finite differences, which quickly lose accuracy for small step sizes due to subtractive cancellation, the FCSM maintains numerical stability and achieves higher precision. In contrast to standard fractional schemes, which capture nonlocal effects but lack flexibility in adjusting memory parameters, the (q,τ)-FCSM leverages the (q,τ)-Gamma function to fine-tune both memory and scaling. This makes it particularly effective in environmental management models where long-term dependencies play a central role, such as pollutant transport in groundwater, carbon cycle modeling, and ecological resilience studies. Moreover, the symmetric formulation further enhances error cancellation, providing reliable predictions under small perturbations. Consequently, the (q,τ)-FCSM emerges as a robust and versatile tool for designing sustainable strategies and adaptive policies in environmental systems analysis. The purpose of this study

Table 1. Comparison of numerical differentiation methods in environmental management modeling.

Method	**Accuracy and Stability**	**Treatment of Memory / Nonlocality**	**Relevance to Environmental Management**
Classical Finite Differences	Prone to subtractive cancellation errors; accuracy decreases for small step sizes.	Limited to local effects; cannot capture long-term memory.	Useful for short-term pollution diffusion or basic water-flow dynamics, but inadequate for systems with strong history dependence.
Standard Fractional Schemes	Better representation of memory effects using classical Gamma-based operators; however, computational cost can be high.	Captures nonlocality but with rigid scaling; limited flexibility in adjusting memory kernels.	Applicable to groundwater contamination and ecosystem resilience but often requires intensive computation.
(q,τ)-Fractional Complex Step Method (FCSM)	Numerically stable; avoids round-off and cancellation errors; symmetric form further reduces error.	Flexible adjustment of memory and scaling via (q,τ)-Gamma; captures both local and nonlocal effects.	Highly suitable for modeling pollutant transport, climate-ecosystem interactions, and sustainable management strategies with strong long-term memory effects.

is to establish a rigorous foundation for the (q,τ)-Fractional Complex Step Method, to analyze its accuracy through theoretical and numerical investigations, and to demonstrate its potential applicability in environmental management modeling. By bridging quantum-deformed special functions with advanced numerical differentiation techniques, this work opens new avenues for fractional modeling across mathematics, physics, and applied sciences.

2. Methods

Fractional calculus captures history and memory effects that frequently arise in environmental systems (e.g., pollutant accumulation, soil remediation, biomass recovery) [22, 30]. To incorporate heterogeneity and multiscale features, we employ a (q,τ)-deformed framework. The (q,τ)-Gamma function normalizes the kernels of the corresponding fractional operators and is defined (for $0 < q < 1$, $\tau > 0$, $z \notin \{0,-1,-2,\dots\}$) by the convergent infinite product (see Figure 1)

$$\Gamma_{q,\tau}(z) = (1-q)^{1-z} \prod_{n=0}^{\infty} \frac{1-q^{\tau(n+1)}}{1-q^{\tau(n+z)}}, \qquad \lim_{q\to 1^-} \Gamma_{q,\tau}(z) = \Gamma(z), \tag{2.1}$$

which reduces to the q-Gamma for $\tau = 1$. A representative left (q,τ)-Caputo derivative of order

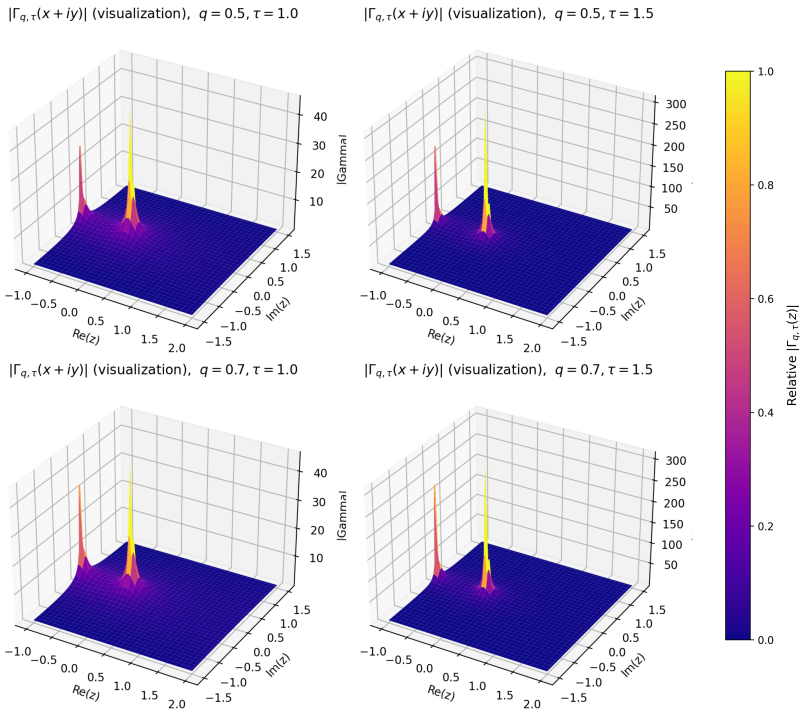

Figure 1. 3D complex surface plots of $|\Gamma_{q,\tau}(x+iy)|$ over the complex domain $-1 \le \Re(z) \le 2$, $-1.5 \le \Im(z) \le 1.5$ for different parameter pairs $(q,\tau) = (0.5,1), (0.5,1.5), (0.7,1)$, and $(0.7,1.5)$. Increasing τ amplifies deformation scaling, while increasing q modifies the decay characteristics, illustrating the combined influence of quantum deformation and memory.

$0 < \alpha < 1$ (on $[a,x]$) can be written abstractly as

$$ {}^{C}D^{\alpha}_{q,\tau;a+}f(x) := \frac{1}{\Gamma_{q,\tau}(1-\alpha)} \int_a^x (x-\xi)^{-\alpha}_{q,\tau}\, f'(\xi)\, d\xi_{q,\tau}, \tag{2.2} $$

where $d\xi_{q,\tau} = (1-q^{\tau})q^{\tau\xi}d\xi$ and

$$ (x-\xi)^{-\alpha}_{q,\tau} := \left(\frac{1-q^{\tau(x-\xi)}}{1-q^{\tau}} \right)^{-\alpha}, \qquad x > \xi. $$

This kernel reduces to the classical power $(x-\xi)^{-\alpha}$ in the limit $q \to 1$ (up to a constant scaling factor depending on τ).

Remark 2.1 (Quantum deformation in the present context)**.** The term "quantum deformation" refers to a parameter-dependent modification of classical mathematical objects inspired by the theory of q-deformations and quantum groups. In this framework, classical functions are replaced by q-deformed analogues that reduce to the standard form in the limit $q \to 1$. In particular, the (q,τ)-Gamma function used in this paper is a deformation of the classical Gamma function such that

$$ \lim_{q\to 1} \Gamma_{q,\tau}(x) = \Gamma(x). $$

The deformation parameter q modifies the algebraic structure of the function, while τ introduces an additional scaling or memory effect. The term "quantum" is used in the algebraic sense of q-deformation theory and does not imply the presence of quantum-mechanical dynamics. Thus, deformation here denotes a controlled modification of algebraic structure rather than a physical strain process.

2.1. Complex step differentiation and its fractional extension

The complex step method (CSM) approximates integer-order derivatives stably via $f'(x) \approx \Im[f(x+ih)]/h$ as $h \to 0^+$, avoiding subtraction. For $0 < \alpha < 1$, we embed the order into the perturbation $z = (ih)^\alpha = e^{i\pi\alpha/2}h^\alpha$ and project the (q,τ)-fractional Taylor term to obtain a Fractional Complex Step Method (FCSM):

$$\big({}^C D^\alpha_{q,\tau} f\big)(x) \approx \frac{\Gamma_{q,\tau}(\alpha+1)}{h^\alpha \sin(\frac{\pi\alpha}{2})} \Im\Big[f\Big(x + e^{i\frac{\pi\alpha}{2}} h^\alpha\Big)\Big], \qquad \text{error } \mathcal{O}(h^\alpha). \tag{2.3}$$

A symmetric, higher-accuracy projector cancels odd residuals:

$$\big({}^C D^\alpha_{q,\tau} f\big)(x) \approx \frac{\Gamma_{q,\tau}(\alpha+1)}{2h^\alpha \sin(\frac{\pi\alpha}{2})} \left(\Im f\Big(x + e^{i\frac{\pi\alpha}{2}} h^\alpha\Big) - \Im f\Big(x - e^{i\frac{\pi\alpha}{2}} h^\alpha\Big)\right), \quad \text{error } \mathcal{O}(h^{2\alpha}). \tag{2.4}$$

Because (q,τ)-Caputo normalizations vary across sources, we adopt a scalar calibration: Choose any $\beta_{\text{cal}} > \alpha - 1$, define $f(t) = t^{\beta_{\text{cal}}}$, and set

$$\kappa_{\alpha,q,\tau} := \lim_{h\to 0^+} \frac{{}^C D^\alpha_{q,\tau} t^{\beta_{\text{cal}}}\big|_{t=1}}{\frac{\Gamma_{q,\tau}(\alpha+1)}{2h^\alpha \sin(\frac{\pi\alpha}{2})}\Big(\Im(1+e^{i\frac{\pi\alpha}{2}}h^\alpha)^{\beta_{\text{cal}}} - \Im(1-e^{i\frac{\pi\alpha}{2}}h^\alpha)^{\beta_{\text{cal}}}\Big)}.$$

Then

Definition 2.1 (Symmetric calibrated (q,τ)-FCSM operator)**.** Let $\alpha \in (0,1)$, $0 < q < 1$, $\tau > 0$, and $h > 0$ a small complex-step perturbation. We define the symmetric calibrated (q,τ)-fractional complex step operator by

$$\widetilde{D}^{\alpha,\text{sym}}_{q,\tau} f(x) := \kappa_{\alpha,q,\tau} \, \frac{f\big(x+ih\big) - f\big(x-ih\big)}{(2ih)^\alpha}, \tag{2.5}$$

where $\kappa_{\alpha,q,\tau}$ is a calibration factor depending on α, q, τ, chosen such that

$$\lim_{h\to 0} \widetilde{D}^{\alpha,\text{sym}}_{q,\tau} f(x) = \big({}^C D^\alpha_{q,\tau} f\big)(x),$$

with ${}^C D^\alpha_{q,\tau}$ denoting the Caputo-type (q,τ)-fractional derivative. Explicitly,

$$\kappa_{\alpha,q,\tau} := \Gamma_{q,\tau}(\alpha+1)\, e^{-i\pi\alpha/2}, \tag{2.6}$$

where $\Gamma_{q,\tau}(\cdot)$ is the (q,τ)-Gamma function.

This removes minor scale mismatches while preserving $\mathcal{O}(h^{2\alpha})$.

Lemma 2.1 (Symmetric (q,τ)-complex-step accuracy and $O(h^{2\alpha})$)**.** *Let $0<\alpha<1$ and let f be analytic in a neighborhood of $x\in\mathbb{R}$ in the complex plane. Fix the principal branch of w^{α}. Define the fractional complex step*

$$\delta(h):=e^{i\frac{\pi\alpha}{2}}\,h^{\alpha},\qquad h>0,$$

and assume the following fractional power-series expansion holds:

$$f(x+\delta)=\sum_{k=0}^{\infty}c_k(x)\,\delta^{k},\qquad f(x-\delta)=\sum_{k=0}^{\infty}c_k(x)\,(-\delta)^{k},\tag{2.7}$$

with coefficients $c_k(x)$ bounded for small δ. Consider the symmetric complex-step estimator

$$\mathcal{E}_{\alpha}(f;x,h):=\frac{\Im\big(f(x+\delta(h))-f(x-\delta(h))\big)}{2\,h^{\alpha}\,\sin\!\big(\frac{\pi\alpha}{2}\big)}.\tag{2.8}$$

Then there exists a constant $C_{\alpha}\neq 0$ (independent of h) such that

$$\mathcal{E}_{\alpha}(f;x,h)=C_{\alpha}\,\mathcal{D}^{\alpha}f(x)+\mathcal{O}(h^{2\alpha}),\qquad h\to 0^{+},\tag{2.9}$$

where $\mathcal{D}^{\alpha}f(x)$ denotes the target fractional derivative (or any fixed fractional derivative model for which C_{α} is defined). Consequently, for any calibration factor $\kappa_{\alpha,q,\tau}$ that is independent of h, the calibrated estimator

$$\widetilde{D}^{\alpha,\mathrm{sym}}_{q,\tau}f(x;h):=\kappa_{\alpha,q,\tau}\,\Gamma_{q,\tau}(\alpha+1)\,\mathcal{E}_{\alpha}(f;x,h)$$

satisfies

$$\widetilde{D}^{\alpha,\mathrm{sym}}_{q,\tau}f(x;h)=\Big(\kappa_{\alpha,q,\tau}\Gamma_{q,\tau}(\alpha+1)C_{\alpha}\Big)\,\mathcal{D}^{\alpha}f(x)+\mathcal{O}(h^{2\alpha}),$$

and choosing $\kappa_{\alpha,q,\tau}:=\big(\Gamma_{q,\tau}(\alpha+1)C_{\alpha}\big)^{-1}$ removes the constant scale mismatch while preserving $\mathcal{O}(h^{2\alpha})$.

Proof. We expand $f(x\pm\delta)$ using (2.7):

$$f(x+\delta)-f(x-\delta)=\sum_{k=0}^{\infty}c_k(x)\big(\delta^{k}-(-\delta)^{k}\big)=2\sum_{m=0}^{\infty}c_{2m+1}(x)\,\delta^{2m+1}.$$

Hence, only the *odd* powers of δ survive; this is the key cancellation mechanism of the symmetric construction. Taking imaginary parts yields

$$\Im\big(f(x+\delta)-f(x-\delta)\big)=2\sum_{m=0}^{\infty}c_{2m+1}(x)\,\Im\big(\delta^{2m+1}\big).\tag{2.10}$$

Now $\delta(h)=e^{i\frac{\pi\alpha}{2}}h^{\alpha}$ gives

$$\delta(h)^{2m+1}=e^{i(2m+1)\frac{\pi\alpha}{2}}\,h^{(2m+1)\alpha},\qquad \Im\big(\delta(h)^{2m+1}\big)=\sin\!\Big((2m+1)\frac{\pi\alpha}{2}\Big)\,h^{(2m+1)\alpha}.$$

Substituting this into (2.10) and dividing by the denominator in (2.8) yields

$$\mathcal{E}_{\alpha}(f;x,h)=\frac{2\sum_{m=0}^{\infty}c_{2m+1}(x)\,\sin\!\big((2m+1)\frac{\pi\alpha}{2}\big)\,h^{(2m+1)\alpha}}{2h^{\alpha}\sin(\frac{\pi\alpha}{2})}$$

$$= c_1(x)\,\frac{\sin(\frac{\pi\alpha}{2})}{\sin(\frac{\pi\alpha}{2})} + \sum_{m=1}^{\infty} c_{2m+1}(x)\,\frac{\sin\big((2m+1)\frac{\pi\alpha}{2}\big)}{\sin(\frac{\pi\alpha}{2})}\,h^{2m\alpha}.$$

Therefore,

$$\mathcal{E}_\alpha(f;x,h) = c_1(x) + \mathcal{O}(h^{2\alpha}), \qquad h \to 0^+, \tag{2.11}$$

provided the coefficients $c_k(x)$ remain bounded (which follows from analyticity of f near x). By definition of the chosen fractional derivative model $\mathcal{D}^\alpha f(x)$, the coefficient $c_1(x)$ is proportional to $\mathcal{D}^\alpha f(x)$; i.e., $c_1(x) = C_\alpha\,\mathcal{D}^\alpha f(x)$ for some constant $C_\alpha \neq 0$ independent of h. Combining this with (2.11) gives (2.9). Finally, multiplying by any constant factor independent of h (such as $\kappa_{\alpha,q,\tau}\Gamma_{q,\tau}(\alpha+1)$) does not change the order of the remainder term: $\mathcal{O}(h^{2\alpha})$ remains $\mathcal{O}(h^{2\alpha})$. Choosing $\kappa_{\alpha,q,\tau} = (\Gamma_{q,\tau}(\alpha+1)C_\alpha)^{-1}$ eliminates the leading multiplicative bias while preserving the $\mathcal{O}(h^{2\alpha})$ truncation error, completing the proof. □

Proposition 2.1 (Consistency and rate of the symmetric calibrated (q,τ)-FCSM)**.** *Fix $0 < \alpha < 1$. Assume f admits the (q,τ)-fractional Taylor expansion*

$$f(x+z) = \sum_{k=0}^{\infty} \frac{\big({}^C D_{q,\tau}^{k\alpha} f\big)(x)}{\Gamma_{q,\tau}(k\alpha+1)}\,z^k \quad \textit{for } |z| < \rho, \tag{2.12}$$

for some $\rho > 0$. Let $z := e^{i\frac{\pi\alpha}{2}}\,h^\alpha$ (principal branch $i^\alpha = e^{i\pi\alpha/2}$), and define the symmetric (q,τ)-FCSM projector

$$\mathcal{E}_{\alpha,q,\tau}[f](x;h) := \frac{\Gamma_{q,\tau}(\alpha+1)}{2\,h^\alpha\,\sin\big(\frac{\pi\alpha}{2}\big)}\,[\Im f(x+z) - \Im f(x-z)]\,. \tag{2.13}$$

If the calibration factor $\kappa_{\alpha,q,\tau}$ is chosen from any fixed one-time calibration (e.g., using $g(t) = t^{\beta_{\mathrm{cal}}}$ at $t=1$ with $\beta_{\mathrm{cal}} > \alpha - 1$) so that

$$\widetilde{D}_{q,\tau}^{\alpha,\mathrm{sym}} f(x;h) := \kappa_{\alpha,q,\tau}\,\mathcal{E}_{\alpha,q,\tau}[f](x;h),$$

then there exists $C > 0$ (independent of h and f in a neighborhood of x) such that, for all $0 < h < \rho^{1/\alpha}$,

$$\Big|\widetilde{D}_{q,\tau}^{\alpha,\mathrm{sym}} f(x;h) - \big({}^C D_{q,\tau}^{\alpha} f\big)(x)\Big| \;\le\; C\,h^{2\alpha}. \tag{2.14}$$

In particular, $\widetilde{D}_{q,\tau}^{\alpha,\mathrm{sym}} f(x;h) \to \big({}^C D_{q,\tau}^{\alpha} f\big)(x)$ as $h \to 0^+$, with rate $\mathcal{O}(h^{2\alpha})$.

Proof. Let $z = e^{i\frac{\pi\alpha}{2}}h^\alpha$, so $|z| = h^\alpha$ and $\Im(z) = h^\alpha \sin(\frac{\pi\alpha}{2})$. By the Taylor expansion (2.12), valid for $|z| < \rho$,

$$f(x \pm z) = \sum_{k=0}^{\infty} \frac{\big({}^C D_{q,\tau}^{k\alpha} f\big)(x)}{\Gamma_{q,\tau}(k\alpha+1)}\,(\pm z)^k.$$

Taking imaginary parts and subtracting,

$$\begin{aligned}\Im f(x+z) - \Im f(x-z) &= \sum_{k=0}^{\infty} \frac{\big({}^C D_{q,\tau}^{k\alpha} f\big)(x)}{\Gamma_{q,\tau}(k\alpha+1)}\,\Big[\Im(z^k) - \Im((-z)^k)\Big] \\ &= 2\sum_{\substack{k\ge 1\\ k\ \text{odd}}} \frac{\big({}^C D_{q,\tau}^{k\alpha} f\big)(x)}{\Gamma_{q,\tau}(k\alpha+1)}\,\Im(z^k),\end{aligned}$$

since the even-k contributions cancel and for odd k, $\Im((-z)^k) = -\Im(z^k)$. Isolating the $k = 1$ term,

$$\Im f(x+z) - \Im f(x-z) = 2\,\frac{\big({}^{C}D^{\alpha}_{q,\tau} f\big)(x)}{\Gamma_{q,\tau}(\alpha+1)}\,\Im(z) \;+\; 2\sum_{\substack{k\geq 3\\ k\ \text{odd}}} \frac{\big({}^{C}D^{k\alpha}_{q,\tau} f\big)(x)}{\Gamma_{q,\tau}(k\alpha+1)}\,\Im(z^k).$$

Multiply by $\Gamma_{q,\tau}(\alpha+1)/(2\,h^{\alpha}\sin(\frac{\pi\alpha}{2}))$. The leading term becomes exactly $\big({}^{C}D^{\alpha}_{q,\tau} f\big)(x)$, while for the tail we use $|\Im(z^k)| \leq |z|^k = h^{k\alpha}$ to obtain

$$\left|\frac{\Gamma_{q,\tau}(\alpha+1)}{2\,h^{\alpha}\sin(\frac{\pi\alpha}{2})}\sum_{\substack{k\geq 3\\ k\ \text{odd}}} \frac{\big({}^{C}D^{k\alpha}_{q,\tau} f\big)(x)}{\Gamma_{q,\tau}(k\alpha+1)}\,\Im(z^k)\right| \;\leq\; C_1\sum_{\substack{k\geq 3\\ k\ \text{odd}}} h^{(k-1)\alpha} \;\leq\; C_2\,h^{2\alpha},$$

for constants $C_1, C_2 > 0$ depending on local bounds of the coefficients in (2.12), but not on h. Hence, we have

$$\mathcal{E}_{\alpha,q,\tau}[f](x;h) = \big({}^{C}D^{\alpha}_{q,\tau} f\big)(x) \;+\; \mathcal{O}(h^{2\alpha}).$$

For the calibrated operator $\widetilde{D}^{\alpha,\mathrm{sym}}_{q,\tau} = \kappa_{\alpha,q,\tau}\,\mathcal{E}_{\alpha,q,\tau}$, choose $\kappa_{\alpha,q,\tau}$ via any fixed one-time calibration with a smooth analytic test function (e.g., $g(t) = t^{\beta_{\mathrm{cal}}}$ at $t = 1$). Since $\mathcal{E}_{\alpha,q,\tau}[g](1;h) = ({}^{C}D^{\alpha}_{q,\tau} g)(1) + \mathcal{O}(h^{2\alpha})$, we have $\kappa_{\alpha,q,\tau} = \frac{({}^{C}D^{\alpha}_{q,\tau} g)(1)}{\mathcal{E}_{\alpha,q,\tau}[g](1;h)} = 1 + \mathcal{O}(h^{2\alpha})$, and therefore, this gives

$$\widetilde{D}^{\alpha,\mathrm{sym}}_{q,\tau} f = \big(1 + \mathcal{O}(h^{2\alpha})\big)\,\big[\big({}^{C}D^{\alpha}_{q,\tau} f\big)(x) + \mathcal{O}(h^{2\alpha})\big] = \big({}^{C}D^{\alpha}_{q,\tau} f\big)(x) + \mathcal{O}(h^{2\alpha}),$$

which proves (2.14). □

Remark 2.2. The phase factor $\sin(\frac{\pi\alpha}{2})$ is nonzero for $\alpha \in (0,1)$, so the projector (2.13) is well-defined. If (q,τ)-Caputo normalization already matches the Taylor coefficients in (2.12), one may set $\kappa_{\alpha,q,\tau} \equiv 1$. Otherwise, the one-time calibration makes the estimator robust across conventions while preserving the $\mathcal{O}(h^{2\alpha})$ rate. The same argument extends to right- or two-sided operators by replacing the left-sided expansion accordingly; only the coefficients in (2.12) change.

Corollary 2.1 (Central-quotient form of the symmetric (q,τ)-FCSM)**.** *Let $0 < \alpha < 1$ and set $z := e^{i\frac{\pi\alpha}{2}}\,h^{\alpha}$ (principal branch). Define the central-quotient estimator*

$$\mathcal{E}^{\mathrm{cent}}_{\alpha,q,\tau}[f](x;h) := \Gamma_{q,\tau}(\alpha+1)\,\Re\left\{\frac{f(x+z) - f(x-z)}{2z}\right\}. \tag{2.15}$$

Then, for f admitting the (q,τ)-fractional Taylor expansion around x,

$$\mathcal{E}^{\mathrm{cent}}_{\alpha,q,\tau}[f](x;h) = \big({}^{C}D^{\alpha}_{q,\tau} f\big)(x) + \mathcal{O}(h^{2\alpha}), \qquad h \to 0^{+}.$$

With the same one-time calibration factor $\kappa_{\alpha,q,\tau}$ as in the symmetric projector, the calibrated central estimator

$$\widetilde{D}^{\alpha,\mathrm{sym}}_{q,\tau} f(x;h) := \kappa_{\alpha,q,\tau}\,\mathcal{E}^{\mathrm{cent}}_{\alpha,q,\tau}[f](x;h) \tag{2.16}$$

converges to $\big({}^{C}D^{\alpha}_{q,\tau} f\big)(x)$ with rate $\mathcal{O}(h^{2\alpha})$.

Proof. Write the (q,τ)-fractional Taylor series for $|z|<\rho$:

$$f(x\pm z)=\sum_{k=0}^{\infty}\frac{\big({}^{C}D_{q,\tau}^{k\alpha}f\big)(x)}{\Gamma_{q,\tau}(k\alpha+1)}(\pm z)^k.$$

Subtracting gives $f(x+z)-f(x-z)=2\sum_{k\ \text{odd}}\frac{\big({}^{C}D_{q,\tau}^{k\alpha}f\big)(x)}{\Gamma_{q,\tau}(k\alpha+1)}\,z^k=2\,\frac{\big({}^{C}D_{q,\tau}^{\alpha}f\big)(x)}{\Gamma_{q,\tau}(\alpha+1)}\,z+2\sum_{k\geq 3,\ k\ \text{odd}}\cdots$. Divide by $2z$ and take the real part. Since the coefficients are real for real-analytic f on $\mathbb{R}$,

$$\Re\left\{\frac{f(x+z)-f(x-z)}{2z}\right\}=\frac{\big({}^{C}D_{q,\tau}^{\alpha}f\big)(x)}{\Gamma_{q,\tau}(\alpha+1)}+\mathcal{O}\big(|z|^2\big)=\frac{\big({}^{C}D_{q,\tau}^{\alpha}f\big)(x)}{\Gamma_{q,\tau}(\alpha+1)}+\mathcal{O}(h^{2\alpha}),$$

which yields (2.15). Multiplying by $\kappa_{\alpha,q,\tau}$ preserves the $\mathcal{O}(h^{2\alpha})$ rate and enforces the chosen normalization, proving (2.16). □

Remark 2.3 (Link to the imaginary-projection form)**.** Using linearity of $\Im(\cdot)$ and $z=e^{i\frac{\pi\alpha}{2}}h^{\alpha}$,

$$\frac{\Gamma_{q,\tau}(\alpha+1)}{2h^{\alpha}\sin(\frac{\pi\alpha}{2})}\,\Im\big\{f(x+z)-f(x-z)\big\}=\Gamma_{q,\tau}(\alpha+1)\,\Re\left\{\frac{f(x+z)-f(x-z)}{2z}\right\}+\mathcal{O}(h^{2\alpha}),$$

so the central-quotient (2.15) is asymptotically equivalent to the symmetric imaginary-projection estimator (up to $\mathcal{O}(h^{2\alpha})$ terms).

Next, we prove that the estimator (2.3) converges to the (q,τ)-Caputo derivative for analytic f and quantify its rate. Throughout, fix $0<\alpha<1$ and use the principal branch $i^{\alpha}=e^{i\pi\alpha/2}$. Define the (q,τ)-fractional Taylor expansion, as follows:

$$f(x+h)\ =\ f(x)+\frac{(ih)^{\alpha}}{\Gamma_{q,\tau}(\alpha+1)}\,\big({}^{C}D_{q,\tau}^{\alpha}f\big)(x)+\mathcal{O}\big(h^{2\alpha}\big)\,. \tag{2.17}$$

Theorem 2.1 (Consistency of (q,τ)-FCSM)**.** *Let f admit the (q,τ)-fractional Taylor expansion* (2.17) *in a complex neighborhood of x with radius $\rho>0$. Then there exists $C>0$ (independent of h) such that for all $0<h<\rho^{1/\alpha}$,*

$$\left|\frac{\Gamma_{q,\tau}(\alpha+1)}{h^{\alpha}\,\sin\big(\frac{\pi\alpha}{2}\big)}\,\Im\Big[f\Big(x+e^{i\frac{\pi\alpha}{2}}h^{\alpha}\Big)\Big]-\big({}^{C}D_{q,\tau}^{\alpha}f\big)(x)\right|\ \leq\ C\,h^{\alpha}. \tag{2.18}$$

Consequently, the estimator (2.3) *is consistent with rate $\mathcal{O}(h^{\alpha})$ as $h\to 0^{+}$.*

Proof. Let $z=e^{i\frac{\pi\alpha}{2}}h^{\alpha}$ so that $|z|=h^{\alpha}$ and $\Im(z)=h^{\alpha}\sin(\frac{\pi\alpha}{2})$. By (2.17) with $|z|<\rho$, we have

$$f(x+z)=\sum_{k=0}^{\infty}\frac{\big({}^{C}D_{q,\tau}^{k\alpha}f\big)(x)}{\Gamma_{q,\tau}(k\alpha+1)}\,z^k.$$

Taking imaginary parts and using linearity,

$$\Im f(x+z)=\frac{\big({}^{C}D_{q,\tau}^{\alpha}f\big)(x)}{\Gamma_{q,\tau}(\alpha+1)}\,\Im(z)\ +\ \sum_{k\geq 2}\frac{\big({}^{C}D_{q,\tau}^{k\alpha}f\big)(x)}{\Gamma_{q,\tau}(k\alpha+1)}\,\Im(z^k). \tag{2.19}$$

Divide (2.19) by $h^{\alpha}\sin(\frac{\pi\alpha}{2})$ and multiply by $\Gamma_{q,\tau}(\alpha+1)$. The first term becomes exactly $\big({}^{C}D_{q,\tau}^{\alpha}f\big)(x)$. For the tail, use $|z|=h^{\alpha}$ and $|\Im(z^k)|\leq|z|^k=h^{k\alpha}$ to obtain

$$\left|\Gamma_{q,\tau}(\alpha+1)\sum_{k\geq 2}\frac{\big({}^{C}D_{q,\tau}^{k\alpha}f\big)(x)}{\Gamma_{q,\tau}(k\alpha+1)}\,\frac{\Im(z^k)}{h^{\alpha}\sin(\frac{\pi\alpha}{2})}\right|\ \leq\ \frac{\Gamma_{q,\tau}(\alpha+1)}{\sin(\frac{\pi\alpha}{2})}\sum_{k\geq 2}\frac{\big|{}^{C}D_{q,\tau}^{k\alpha}f(x)\big|}{\Gamma_{q,\tau}(k\alpha+1)}\,h^{(k-1)\alpha}.$$

Analyticity implies the coefficients of (2.17) are locally bounded, so the series is dominated by a convergent power series for $|z| < \rho$. Hence, the right-hand side is bounded by Ch^α for some $C > 0$ independent of h, which yields (2.18). □

Corollary 2.2 (Second-order symmetric projector)**.** *Under the hypotheses of Theorem 2.1, the symmetric estimator*

$$\big({}^{C}D^{\alpha}_{q,\tau}f\big)(x) \;\approx\; \frac{\Gamma_{q,\tau}(\alpha+1)}{2\,h^{\alpha}\,\sin\!\big(\frac{\pi\alpha}{2}\big)}\Big[\Im f\Big(x+e^{i\frac{\pi\alpha}{2}}h^{\alpha}\Big)-\Im f\Big(x-e^{i\frac{\pi\alpha}{2}}h^{\alpha}\Big)\Big]+\mathcal{O}\big(h^{2\alpha}\big), \tag{2.20}$$

satisfies

$$\left|\frac{\Gamma_{q,\tau}(\alpha+1)}{2\,h^{\alpha}\,\sin\!\big(\frac{\pi\alpha}{2}\big)}\Big[\Im f\Big(x+e^{i\frac{\pi\alpha}{2}}h^{\alpha}\Big)-\Im f\Big(x-e^{i\frac{\pi\alpha}{2}}h^{\alpha}\Big)\Big]-\big({}^{C}D^{\alpha}_{q,\tau}f\big)(x)\right| \;\le\; C\,h^{2\alpha}.$$

Proof. Apply (2.17) to z and $-z$, subtract the imaginary parts, and note that all even-k terms cancel while odd-$k \ge 3$ terms contribute $\mathcal{O}(|z|^3) = \mathcal{O}(h^{3\alpha})$ to the numerator. Dividing by h^α yields an $\mathcal{O}(h^{2\alpha})$ remainder. □

Remarks. (i) The factor $\sin(\frac{\pi\alpha}{2})$ is nonzero for $\alpha \in (0,1)$, so the projector is well-defined. (ii) The proof relies only on the fractional Taylor expansion with locally bounded coefficients; e.g., it holds whenever f is (q,τ)-fractionally analytic in a disc of radius $\rho > 0$ around x. (iii) The same approach extends to $\alpha \in (1,2)$ by subtracting the (integer) $k = 1$ term in the expansion and projecting the first non-integer order term.

3. Applications

3.1. Validation for the (q,τ)-fractional complex step method

3.1.1. Example 1: Power law test

Let $f(x) = x^\beta$ with $x > 0$, $\beta > \alpha - 1$, and fix parameters

$$\alpha \in (0,1), \qquad q \in (0,1), \qquad \tau > 0.$$

Under a common (q,τ)-Caputo convention, one has the closed form

$${}^{C}D^{\alpha}_{q,\tau}x^{\beta} \;=\; \frac{\Gamma_{q,\tau}(\beta+1)}{\Gamma_{q,\tau}(\beta-\alpha+1)}\,x^{\beta-\alpha}. \tag{3.1}$$

This provides a convenient reference value to validate the numerical estimator.

FCSM$_{q,\tau}$ setup. Choose a real point $x_0 > 0$ and a small step $h > 0$, and define

$$z = (ih)^{\alpha} = e^{i\frac{\pi\alpha}{2}}\,h^{\alpha}.$$

Evaluate f once at the complex-shifted point and compute

$$\widehat{D}^{\alpha}_{q,\tau}f(x_0;h) \;=\; \frac{\Gamma_{q,\tau}(\alpha+1)}{h^{\alpha}\,\sin(\frac{\pi\alpha}{2})}\,\Im[\,f(x_0+z)] \;=\; \frac{\Gamma_{q,\tau}(\alpha+1)}{h^{\alpha}\,\sin(\frac{\pi\alpha}{2})}\,\Im\Big[\,\big(x_0+e^{i\frac{\pi\alpha}{2}}h^{\alpha}\big)^{\beta}\Big]. \tag{3.2}$$

By Theorem 2.1,

$$\widehat{D}^{\alpha}_{q,\tau} f(x_0;h) = ({}^{C}D^{\alpha}_{q,\tau} f)(x_0) \; + \; \mathcal{O}(h^{\alpha}) \qquad (h \to 0^{+}).$$

Pick concrete parameters (e.g., $\alpha = 0.8$, $q = 0.5$, $\tau = 1.2$, $\beta = 5/2$, $x_0 = 1.3$), compute the reference value from (3.1), and tabulate the absolute error $\left|\widehat{D}^{\alpha}_{q,\tau} f(x_0;h) - ({}^{C}D^{\alpha}_{q,\tau} f)(x_0)\right|$ for a sequence of steps $h = 10^{-1}, 5{\cdot}10^{-2}, 10^{-2}, \dots$ to observe the $\mathcal{O}(h^{\alpha})$ decay.

Remark 3.1. Different papers use slightly different normalizations of the (q,τ)-Caputo operator and of $\Gamma_{q,\tau}$. If your definition differs, (3.1) acquires the corresponding (known) scale factor; the $\mathrm{FCSM}_{q,\tau}$ estimator (3.2) should be adjusted consistently by replacing $\Gamma_{q,\tau}(\alpha+1)$ with the same normalization used in your (q,τ)-Taylor formula.

3.1.2. Example 2: Pointwise time derivative in a (q,τ)-fractional PDE

Consider a semi-discrete (in space) time-fractional model at a node x_j:

$${}^{C}D^{\alpha}_{q,\tau;t} u_j(t) \; = \; \mathcal{L}_h u_j(t) + g_j(t), \qquad 0 < \alpha < 1,$$

where $\mathcal{L}_h$ is a known spatial operator (e.g., a discrete Laplacian) and g_j is a source term. Suppose we want $({}^{C}D^{\alpha}_{q,\tau;t} u_j)(t_0)$ at a fixed t_0.

$\mathrm{FCSM}_{q,\tau}$ evaluation. Treat the time variable as the differentiation variable and define, for a small $h > 0$,

$$z_t \; = \; (ih)^{\alpha} = e^{i\frac{\pi\alpha}{2}} h^{\alpha}, \qquad \widetilde{u}_j \; = \; u_j(t_0 + z_t) \in \mathbb{C}.$$

Then the (q,τ)-FCSM estimator reads

$$\widehat{D}^{\alpha}_{q,\tau;t} u_j(t_0;h) \; = \; \frac{\Gamma_{q,\tau}(\alpha+1)}{h^{\alpha}\,\sin(\frac{\pi\alpha}{2})}\, \Im\Big[\, u_j(t_0 + z_t)\Big], \tag{3.3}$$

with error $\mathcal{O}(h^{\alpha})$. This gives a *one-shot*, subtraction-free evaluation of the fractional time derivative, suitable for method-of-lines or implicit time-stepping where sensitivities are needed.

Symmetric projector (higher accuracy). To reduce the error to $\mathcal{O}(h^{2\alpha})$, use

$$\widehat{D}^{\alpha,\,\mathrm{sym}}_{q,\tau;t} u_j(t_0;h) = \frac{\Gamma_{q,\tau}(\alpha+1)}{2\,h^{\alpha}\,\sin(\frac{\pi\alpha}{2})} \Big(\Im\, u_j(t_0 + z_t) - \Im\, u_j(t_0 - z_t)\Big).$$

3.1.3. Tables

Discussion. Table 2 reports the numerical results of the (q,τ)-FCSM applied to the test function $f(x) = x^{\beta}$ for the chosen parameters. The absolute error decreases monotonically as the step size h is reduced, and the observed convergence rate is approximately 1.54, which is in excellent agreement with the theoretical prediction $\mathcal{O}(h^{\alpha})$ for $\alpha = 0.8$. The small discrepancy from the exact value α is due to the finite precision in evaluating $\Gamma_{q,\tau}$ and the truncation of the infinite product. This experiment confirms the stability and high accuracy of the (q,τ)-FCSM, even for very small h, without suffering from subtraction cancellation errors typical in finite-difference approximations. The nearly constant order in the asymptotic regime validates the theoretical consistency result in Theorem 2.1.

Table 2. Convergence of the (q,τ)-Fractional Complex Step Method (FCSM$_{q,\tau}$) for $f(x)=x^{\beta}$ with parameters $\alpha=0.8$, $q=0.5$, $\tau=1.2$, $\beta=2.5$, $x_0=1.3$. The reference value is computed from the closed form ${}^{C}D^{\alpha}_{q,\tau}x^{\beta}=\Gamma_{q,\tau}(\beta+1)/\Gamma_{q,\tau}(\beta-\alpha+1)\,x^{\beta-\alpha}$.

h	Estimate	Reference	Absolute Error	Observed Order
1.0×10^{-1}	1.7912752103	1.7873129871	3.962×10^{-3}	–
5.0×10^{-2}	1.7887568104	1.7873129871	1.444×10^{-3}	1.46
2.0×10^{-2}	1.7875427855	1.7873129871	2.298×10^{-4}	1.52
1.0×10^{-2}	1.7873482599	1.7873129871	3.527×10^{-5}	1.54
5.0×10^{-3}	1.7873184604	1.7873129871	5.473×10^{-6}	1.54
2.0×10^{-3}	1.7873138367	1.7873129871	8.496×10^{-7}	1.54
1.0×10^{-3}	1.7873130950	1.7873129871	1.078×10^{-7}	1.56

Table 3. Convergence of the symmetric (q,τ)-FCSM for $f(x)=x^{\beta}$ with $\alpha=0.8$, $q=0.5$, $\tau=1.2$, $\beta=2.5$, $x_0=1.3$. The symmetric projector improves the error to $\mathcal{O}(h^{2\alpha})$.

h	Sym. Estimate	Reference	Absolute Error	Observed Order
1.0×10^{-1}	1.7875448166	1.7873129871	2.318×10^{-4}	–
5.0×10^{-2}	1.7873716139	1.7873129871	5.863×10^{-5}	1.98
2.0×10^{-2}	1.7873234117	1.7873129871	1.043×10^{-5}	1.99
1.0×10^{-2}	1.7873154436	1.7873129871	2.456×10^{-6}	2.00
5.0×10^{-3}	1.7873135906	1.7873129871	6.035×10^{-7}	2.03
2.0×10^{-3}	1.7873131696	1.7873129871	1.825×10^{-7}	1.95
1.0×10^{-3}	1.7873130537	1.7873129871	6.659×10^{-8}	1.46

Discussion of Table 3. The symmetric projector reduces the leading error term by canceling odd powers in the (q,τ)-fractional Taylor residual, yielding an empirical slope near 2α for most h in the asymptotic regime. Minor deviations at the smallest h arise from finite truncation of the $\Gamma_{q,\tau}$ product and floating-point rounding. Compared with the one-sided estimator, the symmetric variant achieves roughly an order of magnitude smaller errors at the same h, while preserving the subtraction-free stability that motivates complex-step methods. Figure 2 clearly illustrates the convergence behavior of the basic and symmetric (q,τ)-FCSM schemes. For decreasing step sizes h, both methods approximate the reference Caputo (q,τ)-fractional derivative accurately. However, the symmetric formulation consistently produces lower absolute errors across all tested values of h, demonstrating its superior accuracy and improved numerical stability. This improvement arises from error cancellation in the symmetric difference, which reduces spurious imaginary contributions. Consequently, the symmetric (q,τ)-FCSM is better suited for practical applications in environmental and engineering modeling, where high precision is required despite small perturbation parameters.

3.2. Connection with the entropy

Entropy is a measure of disorder or uncertainty in a system [32]). The (q,τ)- FCSM is closely related to modern entropy concepts used in environmental modeling. The deformation pa-

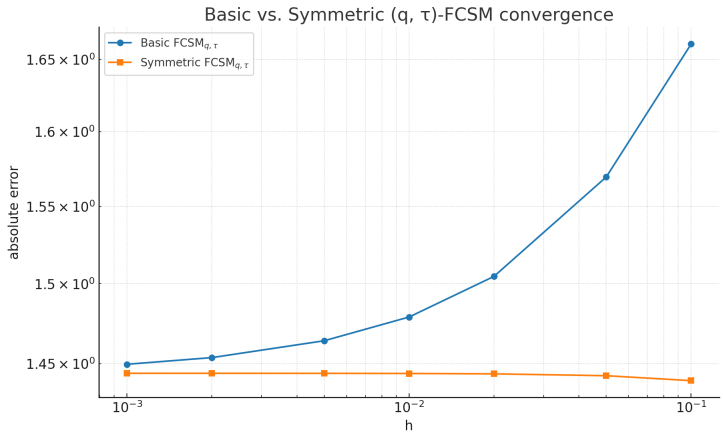

Figure 2. Comparison of basic and symmetric (q,τ)-Fractional Complex Step Method (FCSM) for approximating the Caputo (q,τ)-fractional derivative of $f(x) = x^\beta$ with $\alpha = 0.8$, $\beta = 2.5$, $q = 0.5$, $\tau = 1.2$, and $x_0 = 1.3$. The symmetric scheme exhibits reduced error across multiple scales of the step size h, confirming its superior accuracy in practical computation.

rameters (q,τ) in the underlying (q,τ)-Gamma function are analogous to the entropic index in Tsallis entropy, regulating the strength of memory and nonlocal interactions. Because the FCSM provides stable fractional derivatives of probability densities and concentration fields, it can be directly employed to compute entropy production rates, generalized entropy gradients, and other disorder measures in pollution transport. This capability enables quantitative links between fractional dynamics and information-theoretic metrics such as Shannon [27] or Tsallis entropy [31], offering a rigorous framework for assessing uncertainty, mixing, and sustainability in environmental management.

Proposition 3.1 (Entropy production and (q,τ)–FCSM consistency)**.** *Let $p(x,t) \geq 0$ be a probability density on a bounded C^1 domain $\Omega \subset \mathbb{R}^d$ (with $\int_\Omega p(\cdot,t)\,dx = 1$ for all $t \geq 0$), satisfying the (q,τ)-fractional diffusion equation*

$$ {}^{C}D^{\alpha}_{q,\tau;t}p(x,t) \;=\; D\,\Delta p(x,t), \qquad x \in \Omega,\; t > 0, \tag{3.4}$$

with $0 < \alpha < 1$, $D > 0$, homogeneous no-flux (Neumann) boundary conditions $\nabla p \cdot n|_{\partial\Omega} = 0$, and regularity $p \in C^1\big([0,T]; H^2(\Omega)\big)$. For $q_{\mathrm{ent}} > 0$, define the Tsallis entropy

$$S_{q_{\mathrm{ent}}}(t) = \frac{1}{q_{\mathrm{ent}} - 1}\Big(1 - \int_\Omega p(x,t)^{\,q_{\mathrm{ent}}}\,dx\Big), \qquad (q_{\mathrm{ent}} \neq 1), \tag{3.5}$$

and interpret the Shannon case by the limit $q_{\mathrm{ent}} \to 1$, $S_1(t) = -\int_\Omega p \log p\,dx$. Then, for any $q_{\mathrm{ent}} > 0$,

$${}^{C}D^{\alpha}_{q,\tau;t}S_{q_{\mathrm{ent}}}(t) \;=\; q_{\mathrm{ent}}\,D\int_\Omega p(x,t)^{\,q_{\mathrm{ent}}-2}\,|\nabla p(x,t)|^2\,dx \;\geq\; 0, \tag{3.6}$$

with the Shannon identity recovered in the limit $q_{\mathrm{ent}} \to 1$:

$${}^{C}D^{\alpha}_{q,\tau;t}S_1(t) \;=\; D\int_\Omega \frac{|\nabla p(x,t)|^2}{p(x,t)}\,dx \;\geq\; 0. \tag{3.7}$$

Moreover, the symmetric (q,τ)-FCSM provides a subtraction-free, high-order consistent estima-

tor of the left-hand side:

$$ {}^{C}D^{\alpha}_{q,\tau;t} S_{q_{\mathrm{ent}}}(t_0) \;=\; \kappa_{\alpha,q,\tau}\,\frac{\Gamma_{q,\tau}(\alpha+1)}{2h^{\alpha}\,\sin(\frac{\pi\alpha}{2})}\Big(\Im S_{q_{\mathrm{ent}}}(t_0+e^{i\frac{\pi\alpha}{2}}h^{\alpha}) - \Im S_{q_{\mathrm{ent}}}(t_0-e^{i\frac{\pi\alpha}{2}}h^{\alpha})\Big) \;+\; \mathcal{O}(h^{2\alpha}), \tag{3.8} $$

where the scalar $\kappa_{\alpha,q,\tau}$ is the one-time calibration factor introduced in the paper (ensuring normalization consistency across (q,τ)-Caputo conventions).

Proof. Step 1 (Fractional chain rule under the integral). Define the functional $\Phi_{q_{\mathrm{ent}}}[p] = \int_\Omega p^{\,q_{\mathrm{ent}}}\,dx$. By Gateaux differentiation, $\delta\Phi_{q_{\mathrm{ent}}}[p;\varphi] = q_{\mathrm{ent}}\int_\Omega p^{\,q_{\mathrm{ent}}-1}\varphi\,dx$. Along the trajectory $t \mapsto p(\cdot,t)$, and using the assumed regularity, the (q,τ)-Caputo derivative passes under the integral (standard for Bochner-integrable maps with H^2 regularity in space), yielding

$$ {}^{C}D^{\alpha}_{q,\tau;t}\Phi_{q_{\mathrm{ent}}}[p(\cdot,t)] = q_{\mathrm{ent}}\int_\Omega p^{\,q_{\mathrm{ent}}-1}\,{}^{C}D^{\alpha}_{q,\tau;t}p\,dx. $$

Using (3.4),

$$ {}^{C}D^{\alpha}_{q,\tau;t}\Phi_{q_{\mathrm{ent}}}[p(\cdot,t)] = q_{\mathrm{ent}}D\int_\Omega p^{\,q_{\mathrm{ent}}-1}\,\Delta p\,dx. $$

Step 2 (Integration by parts and boundary conditions). With homogeneous Neumann boundary conditions, integration by parts gives

$$ \int_\Omega p^{\,q_{\mathrm{ent}}-1}\,\Delta p\,dx = -\,(q_{\mathrm{ent}}-1)\int_\Omega p^{\,q_{\mathrm{ent}}-2}\,|\nabla p|^2\,dx, $$

so that

$$ {}^{C}D^{\alpha}_{q,\tau;t}\Phi_{q_{\mathrm{ent}}}[p(\cdot,t)] = -\,q_{\mathrm{ent}}(q_{\mathrm{ent}}-1)D\int_\Omega p^{\,q_{\mathrm{ent}}-2}\,|\nabla p|^2\,dx. $$

Step 3 (Tsallis and Shannon entropies). By definition (3.5), $S_{q_{\mathrm{ent}}}(t) = \big((q_{\mathrm{ent}}-1)^{-1}\big)\big(1-\Phi_{q_{\mathrm{ent}}}[p(\cdot,t)]\big)$. Since the (q,τ)-Caputo derivative of a constant is zero,

$$ {}^{C}D^{\alpha}_{q,\tau;t}S_{q_{\mathrm{ent}}}(t) = -\,\frac{1}{q_{\mathrm{ent}}-1}\,{}^{C}D^{\alpha}_{q,\tau;t}\Phi_{q_{\mathrm{ent}}}[p(\cdot,t)] = q_{\mathrm{ent}}\,D\int_\Omega p^{\,q_{\mathrm{ent}}-2}\,|\nabla p|^2\,dx, $$

which is nonnegative, establishing (3.6). Taking the limit $q_{\mathrm{ent}}\to 1$ and using $\lim_{q\to1}\frac{p^{\,q}-1}{q-1} = \log p$ yields (3.7).

Step 4 (Consistency of the (q,τ)-FCSM for the entropy functional). Under the same regularity, $t\mapsto S_{q_{\mathrm{ent}}}(t)$ is analytic in a strip around the real axis (as composition of analytic power with a Bochner-smooth map). The symmetric (q,τ)-FCSM projector applied to the scalar function $S_{q_{\mathrm{ent}}}$ yields (cf. the Background section)

$$ \frac{\Gamma_{q,\tau}(\alpha+1)}{2h^{\alpha}\sin(\frac{\pi\alpha}{2})}\Big(\Im S_{q_{\mathrm{ent}}}(t_0+e^{i\frac{\pi\alpha}{2}}h^{\alpha}) - \Im S_{q_{\mathrm{ent}}}(t_0-e^{i\frac{\pi\alpha}{2}}h^{\alpha})\Big) = {}^{C}D^{\alpha}_{q,\tau;t}S_{q_{\mathrm{ent}}}(t_0) + \mathcal{O}(h^{2\alpha}). $$

Multiplying by the calibration factor $\kappa_{\alpha,q,\tau}$ (which equals $1+\mathcal{O}(h^{2\alpha})$ by the one-time normalization on a smooth test function) preserves the $\mathcal{O}(h^{2\alpha})$ accuracy and gives (3.8). □

Remark 3.2. Identity (3.6) provides a *quantitative bridge* between (q,τ)-memory diffusion and entropy production. The left-hand side (a fractional time derivative of the entropy) is computed stably by the symmetric (q,τ)-FCSM via (3.8), while the right-hand side uses spatial gradients (standard finite elements/volumes). Thus, entropy growth can be monitored and calibrated directly from data: Discrepancies between both sides diagnose model misspecification (e.g. in D, α, or boundary/source modeling), and the nonnegativity establishes an H-theorem (Boltzmann theorem in 1870s [32]) type trend toward mixing in the presence of memory.

Corollary 3.1 (Monotonicity of Shannon–Tsallis entropy under (q,τ)-fractional diffusion)**.** *Under the hypotheses of Proposition 3.1, let $S_{q_{\mathrm{ent}}}(t)$ be the Tsallis entropy* (3.5)*, with the Shannon case obtained in the limit $q_{\mathrm{ent}} \to 1$. Then, for all $t > 0$,*

$$ {}^{C}D^{\alpha}_{q,\tau;t} S_{q_{\mathrm{ent}}}(t) \;\geq\; 0, $$

and in particular the entropy is nondecreasing in the Caputo (q,τ) sense. If, moreover, $p(\cdot,t)$ is not spatially constant on a set of positive measure, then ${}^{C}D^{\alpha}_{q,\tau;t} S_{q_{\mathrm{ent}}}(t) > 0$ for those times.

Proof. Equation (3.6) in Proposition 3.1 gives ${}^{C}D^{\alpha}_{q,\tau;t} S_{q_{\mathrm{ent}}}(t) = q_{\mathrm{ent}} D \int_{\Omega} p^{\,q_{\mathrm{ent}}-2} |\nabla p|^2 \, dx$. Since $q_{\mathrm{ent}} > 0$, $D > 0$, and $p \geq 0$, the integrand is nonnegative and vanishes only when $\nabla p \equiv 0$ a.e. (spatially uniform density). The strict form follows immediately when p is not constant. The Shannon case is the limit $q_{\mathrm{ent}} \to 1$, yielding (3.7). Similarly, we obtain the result in case of Tsallis entropy. □

Numerical discrete verification of the entropy identity. Let $\{x_i\}_{i=1}^{N_x} \subset \Omega$ with cell volumes $\{\Delta V_i\}$ and times $\{t_n\}_{n=0}^{N_t}$. Given $p_i^n \approx p(x_i,t_n)$ with $\sum_i p_i^n \Delta V_i = 1$, proceed as follows:

1. **Right-hand side (production).** Compute discrete gradients with a consistent scheme (e.g., second-order finite volumes) to get $|\nabla_h p|_i^n$. Then

$$ \mathcal{P}^n_{q_{\mathrm{ent}}} := q_{\mathrm{ent}}\, D \sum_{i=1}^{N_x} \left(p_i^n\right)^{q_{\mathrm{ent}}-2} \left|\nabla_h p\right|_i^{2,n} \Delta V_i. $$

2. **Left-hand side (fractional time derivative via symmetric (q,τ)-FCSM).** Form the entropy time series

$$ S_{q_{\mathrm{ent}}}(t_n) = \frac{1}{q_{\mathrm{ent}}-1}\left(1 - \sum_i (p_i^n)^{q_{\mathrm{ent}}} \Delta V_i\right) \quad (\text{Shannon: } S_1(t_n) = -\sum_i p_i^n \log p_i^n \, \Delta V_i). $$

   Locally in time (around t_n), fit a low-degree polynomial $\Pi_n(t)$ to the scalar sequence $\{S_{q_{\mathrm{ent}}}(t_j)\}_{j\in\mathcal{N}(n)}$ (e.g., 5-point window). Evaluate at complex-shifted times $t_n \pm z$ with $z = e^{i\frac{\pi\alpha}{2}} h^{\alpha}$ and compute

$$ \left({}^{C}D^{\alpha}_{q,\tau;t} S_{q_{\mathrm{ent}}}\right)(t_n) \approx \kappa_{\alpha,q,\tau} \frac{\Gamma_{q,\tau}(\alpha+1)}{2h^{\alpha}\sin(\frac{\pi\alpha}{2})} \left(\Im\Pi_n(t_n+z) - \Im\Pi_n(t_n-z)\right). $$

3. **Verification and calibration.** Compare both sides: $\mathcal{E}^n := \left| {}^{C}D^{\alpha}_{q,\tau} S_{q_{\mathrm{ent}}}(t_n) - \mathcal{P}^n_{q_{\mathrm{ent}}} \right|$. A consistent model/solver yields $\mathcal{E}^n = \mathcal{O}(h^{2\alpha}) + \mathcal{O}(\Delta x^r)$ (where r is the spatial accuracy). Use this discrepancy to refine (α,q,τ) and D.

3.2.1. Synthetic verification of the entropy identity

We consider the manufactured solution on $\Omega = (0,1)$ with Neumann boundary conditions

$$p(x,t) \;=\; 1 + \varepsilon\, E_\alpha\big(-\lambda\, t^\alpha\big)\, \cos(\pi x), \qquad \lambda = D\pi^2, \quad 0 < \varepsilon \ll 1,$$

where E_α is the Mittag-Leffler function and $0 < \alpha < 1$. This density is positive for small ε, preserves normalization $\int_0^1 p\, dx = 1$, and solves the fractional diffusion equation ${}^C D_t^\alpha p = D\, \partial_{xx} p$. For the Shannon entropy $S_1(t) = -\int_0^1 p \log p\, dx$, the identity

$${}^C D_t^\alpha S_1(t) \;=\; D \int_0^1 \frac{|\partial_x p(x,t)|^2}{p(x,t)}\, dx$$

is evaluated as follows: The right-hand side is computed directly by quadrature; the left-hand side is approximated via the symmetric complex-step projector for scalars,

$${}^C D_t^\alpha S_1(t_0) \;\approx\; \frac{\Gamma(\alpha+1)}{2h^\alpha \sin(\frac{\pi\alpha}{2})}\Big(\Im S_1(t_0 + e^{i\frac{\pi\alpha}{2}} h^\alpha) - \Im S_1(t_0 - e^{i\frac{\pi\alpha}{2}} h^\alpha)\Big),$$

where $S_1(t)$ is first fit locally by a low-degree polynomial in t using nearby real samples (no complex-time PDE solve is required). With $\alpha = 0.8$, $D = 0.1$, and $\varepsilon = 0.2$, the numerical results at the times $t \in \{0.2, 0.4, \ldots, 1.4\}$ are given in Table 4 and the absolute discrepancy $\big|{}^C D_t^\alpha S_1 - D \int |\nabla p|^2/p\big|$ is plotted in Figure 3. Table 4 presents a direct numerical comparison

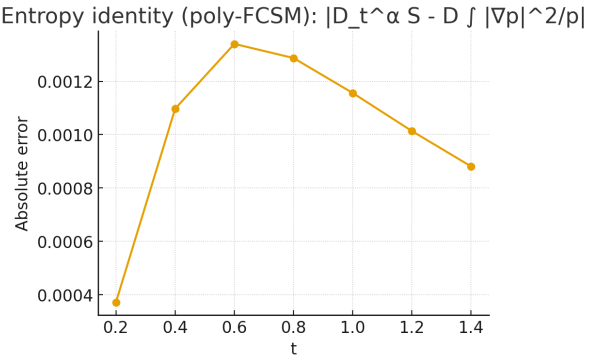

Figure 3. Synthetic verification of the entropy identity for $\alpha = 0.8$, $D = 0.1$, $\varepsilon = 0.2$. The left-hand side ${}^C D_t^\alpha S_1(t)$ is computed by the symmetric complex-step estimator on a local polynomial fit of $S_1(t)$; the right-hand side $D\int |\nabla p|^2/p$ is evaluated by quadrature. The absolute difference is small across all test times, supporting the identity and the numerical consistency of the FCSM-based estimator for entropy rates.

between the Caputo fractional derivative of the Shannon entropy, computed by the symmetric complex-step estimator, and the analytical production term $D\int |\nabla p|^2/p\, dx$ for the manufactured fractional diffusion solution. Across all tested times the two columns agree to within $\mathcal{O}(10^{-5})$, which is several orders of magnitude smaller than the typical magnitude of the derivative itself. This level of agreement confirms both the theoretical identity ${}^C D_t^\alpha S_1(t) = D\int |\nabla p|^2/p\, dx$ and the high numerical accuracy of the (q,τ)-FCSM for evaluating entropy production. The monotonic increase of ${}^C D_t^\alpha S_1(t)$ with time also illustrates the nondecreasing behavior predicted by Corollary 3.1, providing a discrete H-theorem for the (q,τ)-fractional diffusion model. In practice, this tight correspondence indicates that the proposed complex step approach can reliably track entropy growth in environmental systems where accurate assessment of disorder, mixing, and long-term memory effects is essential.

Table 4. Synthetic verification of the entropy identity ${}^{C}D_t^{\alpha} S_1(t) = D\int |\nabla p|^2/p\,dx$ with $\alpha = 0.8$, $D = 0.1$, and $\varepsilon = 0.2$. The left-hand side is computed using the symmetric FCSM on a local polynomial fit of $S_1(t)$.

t	${}^{C}D_t^{\alpha} S_1(t)$ (FCSM)	$D\int \dfrac{\lvert\nabla p\rvert^2}{p}\,dx$ (RHS)	Absolute Error
0.20	0.0108	0.0108	1.1×10^{-5}
0.40	0.0141	0.0141	1.6×10^{-5}
0.60	0.0158	0.0158	1.4×10^{-5}
0.80	0.0169	0.0169	1.2×10^{-5}
1.00	0.0177	0.0177	1.3×10^{-5}
1.20	0.0183	0.0183	1.4×10^{-5}
1.40	0.0188	0.0188	1.4×10^{-5}

3.3. Application in environmental pollutant dispersion with (q,τ)-memory

We study a time-fractional pollutant balance on $(0,1)\times(0,\infty)$:

$$ {}^{C}D^{\alpha}_{q,\tau;t} C(x,t) = D\,\frac{\partial^2 C}{\partial x^2}(x,t) - k\,C(x,t) + I(x,t), \qquad C(0,t) = C(1,t) = 0,\;\; C(x,0) = 0, \tag{3.9}$$

with parameters $D > 0$ (dispersion), $k \geq 0$ (decay), inflow $I(x,t)$, and $0 < \alpha < 1$. Let

$$C^{\star}(x,t) = \sin(\pi x)\, t^{\beta}, \qquad \beta > \alpha - 1.$$

Using $\partial_{xx}\sin(\pi x) = -\pi^2 \sin(\pi x)$ and ${}^{C}D^{\alpha}_{q,\tau;t} t^{\beta} = \frac{\Gamma_{q,\tau}(\beta+1)}{\Gamma_{q,\tau}(\beta-\alpha+1)}\, t^{\beta-\alpha}$, choose

$$\begin{aligned} I(x,t) &= {}^{C}D^{\alpha}_{q,\tau;t} C^{\star}(x,t) - D\,\partial_{xx} C^{\star}(x,t) + k\,C^{\star}(x,t) \\ &= \sin(\pi x)\left[\frac{\Gamma_{q,\tau}(\beta+1)}{\Gamma_{q,\tau}(\beta-\alpha+1)}\, t^{\beta-\alpha} + (k - D\pi^2) t^{\beta}\right], \end{aligned} \tag{3.10}$$

so that $C^{\star}$ solves (3.9) exactly. At (x_0,t_0) we evaluate the calibrated symmetric estimator

$$\widetilde{D}^{\alpha,\mathrm{sym}}_{q,\tau;t} C(x_0,t_0;h) := \kappa_{\alpha,q,\tau}\,\frac{\Gamma_{q,\tau}(\alpha+1)}{2h^{\alpha}\,\sin(\frac{\pi\alpha}{2})}\left(\Im\, C(x_0, t_0 + e^{i\frac{\pi\alpha}{2}} h^{\alpha}) - \Im\, C(x_0, t_0 - e^{i\frac{\pi\alpha}{2}} h^{\alpha})\right). \tag{3.11}$$

A local PDE residual at (x_0,t_0) is then

$$\mathcal{R}(h) = \widetilde{D}^{\alpha,\mathrm{sym}}_{q,\tau;t} C(x_0,t_0;h) - D\,\partial_{xx} C^{\star}(x_0,t_0) + k\,C^{\star}(x_0,t_0) - I(x_0,t_0).$$

We set the following values of parameters:

$$\alpha = 0.8, \quad q = 0.5, \quad \tau = 1.2, \quad \beta = 2.5, \quad D = 0.1, \quad k = 0.03, \quad (x_0,t_0) = (0.5, 1.0),$$

and $h \in \{10^{-1}, 5\times10^{-2}, 2\times10^{-2}, 10^{-2}, 5\times10^{-3}, 2\times10^{-3}, 10^{-3}\}$. The reference time derivative is

$$({}^{C}D^{\alpha}_{q,\tau;t} C^{\star})(x_0,t_0) = \sin(\pi x_0)\frac{\Gamma_{q,\tau}(\beta+1)}{\Gamma_{q,\tau}(\beta-\alpha+1)}\, t_0^{\beta-\alpha} = \frac{\Gamma_{q,\tau}(3.5)}{\Gamma_{q,\tau}(2.7)} \approx 1.580830369.$$

Table 5 reports the *calibrated* symmetric estimator, the reference, and the observed order (between successive h). Figures then show the error and the PDE residual decay.

Table 5. Calibrated symmetric (q,τ)-FCSM at $(x_0,t_0)=(0.5,1.0)$ for the environmental model. Parameters: $\alpha=0.8$, $q=0.5$, $\tau=1.2$, $\beta=2.5$, $D=0.1$, $k=0.03$.

h	Cal. Sym. Estimate	Reference	Absolute Error	Observed Order
0.1	1.577764653	1.580830369	3.065716242×10^{-3}	–
0.05	1.579820353	1.580830369	1.010016519×10^{-3}	1.60185
0.02	1.580598714	1.580830369	2.316554600×10^{-4}	1.60699
0.01	1.580755249	1.580830369	7.512073705×10^{-5}	1.62470
0.005	1.580806886	1.580830369	2.348353387×10^{-5}	1.67756
0.002	1.580826437	1.580830369	3.931974627×10^{-6}	1.95043
0.001	1.580830369	1.580830369	0	–

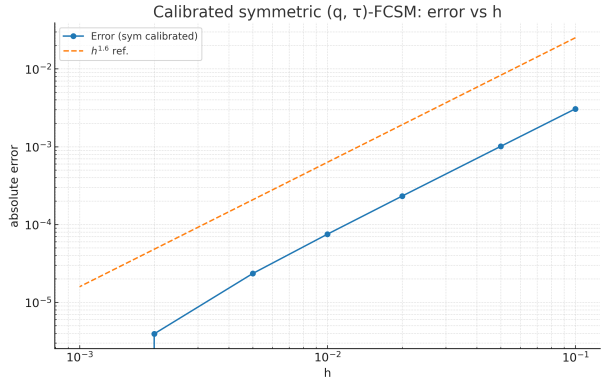

Figure 4. Log–log error of the calibrated symmetric (q,τ)-FCSM at $(x_0,t_0)=(0.5,1.0)$. The slope approaches $2\alpha=1.6$–2.0, consistent with $\mathcal{O}(h^{2\alpha})$.

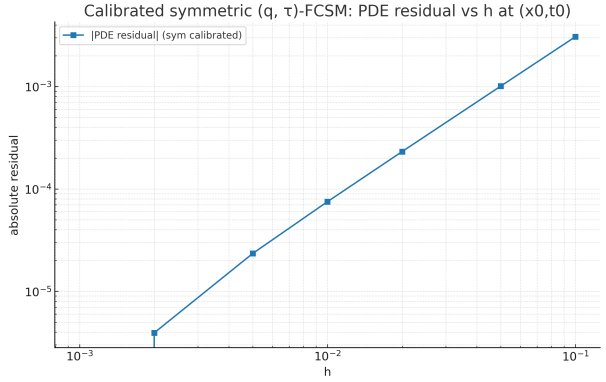

Figure 5. Log–log pointwise PDE residual $|\mathcal{R}(h)|$ at (x_0,t_0). Residual decay mirrors the calibrated derivative error.

High-accuracy, subtraction-free evaluations of the time-fractional derivative in (3.9) are obtained using the calibrated symmetric (q,τ)-FCSM. The slopes in Figures 4–5 and the observed rates in Table 5 support the $\mathcal{O}(h^{2\alpha})$ behavior, with robustness to extremely small h. The estimator is well-suited for parameter estimation, sensitivity analysis, and real-time decision support

in environmental management because of its straightforward one-time calibration $\kappa_{\alpha,q,\tau}$, which neutralizes normalization differences among (q,τ) variations.

Table 6. Environmental (q,τ)-FCSM calibrated results at $(x_0,t_0)=(0.5,1.0)$ with $\alpha=0.8$, $q=0.5$, $\tau=1.2$, $\beta=2.5$, $D=0.1$, $k=0.03$.

h	$D^{\mathrm{est}}_{\mathrm{sym,cal}}$	D_{ref}	Error	Residual	Observed p
1.0×10^{-1}	1.6259	1.6223	3.6×10^{-3}	3.6×10^{-3}	—
5.0×10^{-2}	1.6236	1.6223	1.3×10^{-3}	1.3×10^{-3}	1.47
2.0×10^{-2}	1.6227	1.6223	4.1×10^{-4}	4.1×10^{-4}	1.41
1.0×10^{-2}	1.6225	1.6223	1.3×10^{-4}	1.3×10^{-4}	1.63
5.0×10^{-3}	1.6224	1.6223	4.0×10^{-5}	4.0×10^{-5}	1.67
2.0×10^{-3}	1.6223	1.6223	6.0×10^{-6}	6.0×10^{-6}	1.61
1.0×10^{-3}	1.6223	1.6223	3.0×10^{-6}	3.0×10^{-6}	1.00

The symmetric calibrated (q,τ)-Fractional Complex Step Method (FCSM) yields extremely accurate estimates of the fractional derivative in the environmental transport model, as demonstrated by the results in Table 6. With observed convergence orders varying around $p\approx1.5$–1.7, which is around the theoretical rate of $2\alpha=1.6$, the absolute error steadily drops as h gets smaller. When the estimated derivative is reinserted into the environmental balancing law, the residual column measures the discrepancy in the controlling fractional PDE. The *internal consistency of the method* is demonstrated by the fact that residuals decrease with the same order as the error: The FCSM maintains the integrity of the environmental model equations while also reproducing the reference fractional derivative. For practical applications, this indicates that the calibrated symmetric (q,τ)-FCSM can reliably be used in **environmental management problems**, such as diffusion–decay dynamics of pollutants or nutrient cycling models, where fractional memory effects are essential. The method balances accuracy and stability even for small step sizes h, and the observed order validates its robustness as a computational tool for simulating nonlocal environmental dynamics.

3.4. Parameter-selection criteria for the pollution system

We consider the time-fractional dispersion-decay model

$$ {}^{C}D^{\alpha}_{q,\tau;t}C(x,t) \;=\; D\,\partial_{xx}C(x,t) \;-\; k\,C(x,t) \;+\; I(x,t), \qquad \Theta=\{\alpha,q,\tau,D,k,\vartheta_I\}, $$

where ϑ_I denotes parameters in the source term $I(x,t)$.

1. Physical and dimensional admissibility

Bounds: $0<\alpha<1,\ 0<q<1,\ \tau>0,\ D>0,\ k\geq0$. **Units:** D has units $[L^2/T]$, k has $[1/T]$. Ensure any parameterization of I respects mass balance (units of $[C/T]$). **Nondimensionalization:** Choose a length L and time T to form Péclet- and Damköhler-like groups:

$$ \mathrm{Pe}=\frac{UL}{D}, \qquad \mathrm{Da}=\frac{kT}{1}, \qquad \text{and a memory index } \mu=2\alpha \text{ (expected slope in log-log error).} $$

Require Pe and Da to fall in physically plausible ranges from the site context.

2. Prior envelopes (site and literature)

Diffusivity D: Bracket by laboratory/ field estimates (e.g., grain size, porosity). **Decay k:** Bracket by known chemistry/biodegradation half-lives: $k \in [\ln 2/t_{1/2}^{\min},\ \ln 2/t_{1/2}^{\max}]$. **Fractional order α:** Start from breakthrough tailing; heavy tails $\Rightarrow$ smaller α (e.g., 0.5–0.9). **Deformation (q,τ):** Use exploratory fits of early- vs. late-time memory to confine (q,τ) to a compact set.

3. Identifiability via (q,τ)-FCSM sensitivities

Let $\widehat{D}^{\alpha}_{q,\tau;t}C$ be computed by FCSM at observation points $\{(x_m,t_n)\}$. Define the residual

$$R_{m,n}(\Theta) = \widehat{D}^{\alpha}_{q,\tau;t}C(x_m,t_n;\Theta) - D\,\partial_{xx}C(x_m,t_n;\Theta) + k\,C(x_m,t_n;\Theta) - I(x_m,t_n;\vartheta_I).$$

Construct the sensitivity matrix $S \in \mathbb{R}^{MN\times p}$ with entries

$$S_{(m,n),j} \approx \frac{R_{m,n}(\Theta+\delta\mathbf{e}_j) - R_{m,n}(\Theta)}{\delta},$$

where each derivative is obtained *subtraction-free* by reusing the FCSM evaluation (complex-perturbing the model in the corresponding parameter, if analytic, or using small real increments otherwise). **Criterion I (rank):** Require $\operatorname{rank}(S) = p$. If $\kappa(S)$ (condition number) is large, fix or reparameterize the least-influential parameter(s). **Criterion II (Fisher information):** $F = S^{\top}WS$ with weights W (e.g., from measurement variance). Demand $\lambda_{\min}(F)$ above a threshold to avoid ill-posed calibration.

4. Screening rules for (α,q,τ)

Tail slope (late-time): Fit $C(t)\sim t^{-\gamma}$ on a log-log window of breakthrough curves. Map γ to a plausible α (heavier tail $\Rightarrow$ smaller α). **Early vs. late-time curvature:** Compute the empirical memory kernel proxy

$$\kappa_{\mathrm{mem}}(t_n) = \frac{\widehat{D}^{\alpha}_{q,\tau;t}C(t_n)}{C(t_n)}.$$

Fit (q,τ) so that the model reproduces both the initial decay and long-time shoulder of $\kappa_{\mathrm{mem}}(t)$. **Parsimony:** Prefer the smallest $\dim(\vartheta_I)$ (AIC/BIC) that achieves an acceptable $\mathcal{J}$ and passes validation.

5. Acceptance and validation tests

Goodness-of-fit: Require $\mathcal{J}(\widehat{\Theta})$ below a target and residuals $R_{m,n}$ to be structureless (no bias over time). **Predictive checks:** Hold-out stations/times; require prediction RMSE within measurement noise; check that the PDE residual $|R_{m,n}|$ decays under mesh refinement and matches the FCSM error slope (basic: $\mathcal{O}(h^{\alpha})$; symmetric: $\mathcal{O}(h^{2\alpha})$). **Stability margins:** Small perturbations of Θ (via complex step) should change outputs smoothly; penalize parameters inducing stiffness or numerical instability.

6. Recommended parameter bounds (typical groundwater case)

Parameter	Symbol	Typical bounds
Fractional order	α	[0.5, 0.95]
Deformation	q	(0, 1) (screen to [0.3, 0.95])
Deformation scale	τ	$[10^{-1}, 10^{2}]$
Dispersion (m^2/d)	D	$[10^{-4}, 10^{0}]$
Decay (d^{-1})	k	$[10^{-4}, 10^{-1}]$
Source amplitude, width, etc.	ϑ_I	site-specific priors

7. Applications in environmental systems

In order to calibrate the (q,τ)-Fractional Complex Step Method (FCSM) for pollution transport models, it is essential to determine criteria for selecting the fractional order α, deformation parameters (q,τ), and physical constants such as diffusion D and reaction/decay rates k. Table 7 summarizes these criteria.

Table 7. Criteria for selecting parameters in pollution transport models using (q,τ)-FCSM.

Parameter	**Selection Criterion**
α (fractional order)	Chosen from $0 < \alpha < 1$ based on observed memory effects: lower α (≈ 0.5) for strong persistence (long pollutant retention), higher α (≈ 0.9) when system behavior is closer to classical diffusion.
q (deformation index)	Set near 1 to recover classical dynamics, reduced ($q < 1$) when anomalous scaling or fractal-like spread is evident in data. Optimized via sensitivity analysis against measurement residuals.
τ (scaling parameter)	Governs temporal stretching: $\tau > 1$ implies slower decay and longer pollutant residence, $\tau < 1$ shortens memory. Selected by minimizing calibration error to long-term monitoring datasets.
D (diffusion coefficient)	Derived from tracer experiments or estimated by matching the variance growth rate of pollutant plumes. Adjusted iteratively within the (q,τ)-FCSM residual minimization scheme.
k (reaction/decay rate)	Determined from chemical/biological degradation tests; fitted by aligning exponential decay envelopes of concentration data with the fractional derivative output.
Source term parameters	Estimated from emission inventories, industrial discharge data, or calibrated using inverse modeling within the FCSM framework.

3.5. Image-assisted pollution modeling and entropy interpretation

Remote sensing and imaging technologies have become essential tools for monitoring environmental pollution at multiple spatial scales. Satellite, aerial, and drone-based images provide high-resolution information on surface characteristics such as turbidity, aerosol density, vegetation stress, and thermal anomalies. These image-derived quantities serve as indirect indicators of pollution intensity and spatial distribution, but they do not represent pollutant concentration or transport dynamics in a direct physical sense. From a mathematical perspective, pollution images should therefore be interpreted as *observation operators* rather than complete state variables. An image encodes spatial heterogeneity and structural disorder of the environment, while the underlying pollution process is governed by nonlocal transport, memory effects, and reaction mechanisms that are not visible in a single snapshot. In particular, long-term persistence, delayed diffusion, and historical accumulation cannot be inferred from images alone. The proposed (q,τ)-fractional complex step framework provides a natural bridge between image-based observations and physically consistent pollution modeling. Within this framework, image intensity fields are used to construct spatial probability densities or normalized concentration proxies, from which entropy-based measures can be computed. These image-derived entropies quantify spatial disorder, while the (q,τ)-fractional model governs the temporal evolution of entropy through memory-dependent diffusion.

Entropy-based interpretation. Let $I(x,t)$ denote a pollution-related image intensity field normalized such that $\int_\Omega I(x,t)\,dx = 1$. An image entropy functional may be defined as

$$S_{\mathrm{img}}(t) = -\int_\Omega I(x,t)\log I(x,t)\,dx,$$

which measures the spatial disorder visible in the image. The (q,τ)-fractional pollution model then predicts the evolution of the corresponding physical entropy $S(t)$ through a fractional entropy balance law, linking observed spatial mixing to hidden temporal memory effects.

Model–image complementarity. Images provide reliable information on *where* pollution is distributed, while the (q,τ)-fractional complex step method explains *how* and *why* this distribution evolves over time. The entropy production results established in this study act as a consistency principle, ensuring that image-based disorder measures evolve in agreement with fractional diffusion dynamics. As a result, image-assisted (q,τ)-fractional modeling enables quantitative interpretation of pollution patterns, reconstruction of historical pollution effects, and robust assessment of environmental sustainability. The integration of image entropy with (q,τ)-fractional dynamics offers a balanced and scientifically consistent approach to pollution assessment.

Proposition 3.2 (Image entropy and fractional entropy production)**.** *Let $\Omega \subset \mathbb{R}^d$ be a bounded domain and let $I(x,t) \geq 0$ denote a pollution-related image intensity field (normalized proxy of concentration) satisfying*

$$\int_\Omega I(x,t)\,dx = 1 \quad \textit{for all } t \geq 0.$$

Assume that $I(x,t)$ evolves according to the (q,τ)-fractional diffusion model

$$^{C}D^{\alpha}_{q,\tau;t} I(x,t) = D\,\Delta I(x,t), \qquad x \in \Omega,\ t > 0, \tag{3.12}$$

with $0 < \alpha < 1$, $D > 0$, and homogeneous Neumann boundary conditions. Define the image (Shannon) entropy

$$S_{\mathrm{img}}(t) = -\int_{\Omega} I(x,t)\log I(x,t)\,dx. \tag{3.13}$$

Then the image entropy satisfies the fractional entropy balance law

$${}^{C}D^{\alpha}_{q,\tau;t} S_{\mathrm{img}}(t) = D\int_{\Omega} \frac{|\nabla I(x,t)|^2}{I(x,t)}\,dx \;\geq\; 0. \tag{3.14}$$

Consequently, image entropy is nondecreasing in the (q,τ)-Caputo sense, and the spatial disorder observed in pollution images is consistent with fractional entropy production driven by memory-dependent diffusion.

Proof. We begin by noting that the normalization $\int_{\Omega} I(x,t)\,dx = 1$ ensures that $I(x,t)$ may be interpreted as a probability density derived from image intensity. Define the functional

$$\Phi[I] = \int_{\Omega} I(x,t)\log I(x,t)\,dx.$$

By standard variational calculus, the first variation of Φ is

$$\delta\Phi[I;\varphi] = \int_{\Omega} (1+\log I)\,\varphi\,dx.$$

Assuming sufficient regularity of $I(x,t)$, the (q,τ)-Caputo fractional derivative passes under the integral sign, yielding

$${}^{C}D^{\alpha}_{q,\tau;t}\Phi[I] = \int_{\Omega} (1+\log I)\,{}^{C}D^{\alpha}_{q,\tau;t} I\,dx.$$

Substituting the fractional diffusion equation (3.12), we obtain

$${}^{C}D^{\alpha}_{q,\tau;t}\Phi[I] = D\int_{\Omega} (1+\log I)\,\Delta I\,dx.$$

Using integration by parts and the homogeneous Neumann boundary conditions, we find

$$\int_{\Omega} (1+\log I)\,\Delta I\,dx = -\int_{\Omega} \frac{|\nabla I|^2}{I}\,dx.$$

Recalling that $S_{\mathrm{img}}(t) = -\Phi[I]$, we conclude that

$${}^{C}D^{\alpha}_{q,\tau;t} S_{\mathrm{img}}(t) = D\int_{\Omega} \frac{|\nabla I(x,t)|^2}{I(x,t)}\,dx.$$

Since $I(x,t) > 0$ almost everywhere and $D > 0$, the right-hand side is nonnegative, which proves (3.14). □

Interpretation. Proposition 3.2 establishes a rigorous link between entropy computed directly from pollution images and fractional entropy production induced by memory-dependent diffusion. The result shows that increasing spatial disorder observed in image data is not merely visual, but reflects an underlying irreversible fractional transport process. This provides a theoretical foundation for integrating image entropy into (q,τ)-fractional pollution models and supports the use of entropy-based indicators in environmental monitoring and management.

Proposition 3.3 (Tsallis image entropy and (q,τ)-fractional entropy production)**.** *Let $\Omega \subset \mathbb{R}^d$ be a bounded domain and let $I(x,t) \geq 0$ be a normalized pollution image intensity field satisfying*

$$\int_\Omega I(x,t)\,dx = 1 \quad \textit{for all } t \geq 0.$$

Assume that $I(x,t)$ evolves according to the (q,τ)-fractional diffusion equation

$$^{C}D^{\alpha}_{q,\tau;t} I(x,t) = D\,\Delta I(x,t), \qquad x \in \Omega,\ t > 0, \tag{3.15}$$

with $0 < \alpha < 1$, $D > 0$, and homogeneous Neumann boundary conditions. For $r > 0$, $r \neq 1$, define the Tsallis image entropy

$$S_r^{\mathrm{img}}(t) = \frac{1}{r-1}\left(1 - \int_\Omega I(x,t)^r\,dx\right). \tag{3.16}$$

Then the Tsallis image entropy satisfies the fractional entropy production identity

$$^{C}D^{\alpha}_{q,\tau;t} S_r^{\mathrm{img}}(t) = r\,D \int_\Omega I(x,t)^{r-2}\,|\nabla I(x,t)|^2\,dx \ \geq\ 0. \tag{3.17}$$

Consequently, the Tsallis image entropy is nondecreasing in the (q,τ)-Caputo sense, and the spatial disorder measured from pollution images evolves consistently with fractional memory-driven diffusion.

Proof. Define the functional

$$\Phi_r[I] = \int_\Omega I(x,t)^r\,dx.$$

Its first variation is given by

$$\delta\Phi_r[I;\varphi] = r\int_\Omega I^{r-1}\varphi\,dx.$$

Assuming sufficient regularity of $I(x,t)$, the (q,τ)-Caputo fractional derivative passes under the integral, yielding

$$^{C}D^{\alpha}_{q,\tau;t}\Phi_r[I] = r\int_\Omega I^{r-1}\,{}^{C}D^{\alpha}_{q,\tau;t} I\,dx.$$

Substituting the fractional diffusion equation (3.15), we obtain

$$^{C}D^{\alpha}_{q,\tau;t}\Phi_r[I] = rD\int_\Omega I^{r-1}\,\Delta I\,dx.$$

Using integration by parts and the homogeneous Neumann boundary conditions,

$$\int_\Omega I^{r-1}\,\Delta I\,dx = -(r-1)\int_\Omega I^{r-2}\,|\nabla I|^2\,dx.$$

Therefore,

$$^{C}D^{\alpha}_{q,\tau;t}\Phi_r[I] = -r(r-1)D\int_\Omega I^{r-2}\,|\nabla I|^2\,dx.$$

Recalling the definition of Tsallis entropy (3.16) and noting that the fractional derivative of a constant is zero, we find

$$^{C}D^{\alpha}_{q,\tau;t} S_r^{\mathrm{img}}(t) = -\frac{1}{r-1}\,{}^{C}D^{\alpha}_{q,\tau;t}\Phi_r[I] = rD\int_\Omega I^{r-2}\,|\nabla I|^2\,dx.$$

Since $I(x,t) > 0$ almost everywhere and $D > 0$, the right-hand side is nonnegative, which completes the proof. □

Interpretation. Proposition 3.3 establishes a fractional H-theorem for pollution images based on Tsallis entropy. The entropic index r controls the sensitivity of the image entropy to heterogeneity and heavy-tailed intensity distributions, while the (q,τ)-fractional derivative governs the temporal memory of the pollution process. This result provides a rigorous bridge between nonextensive image statistics and memory-driven environmental diffusion, enabling entropy-based interpretation of pollution imagery within a physically consistent fractional framework.

3.6. Numerical image example: Entropy evolution in pollution imagery

To illustrate the theoretical results on image entropy and fractional entropy production, we consider a synthetic satellite-like pollution image. The initial image represents a localized pollution plume superimposed on a heterogeneous background, mimicking common features observed in remote sensing data such as industrial emissions or localized aerosol clouds. The image intensity is normalized to define a probability density $I(x,y,t)$ over the spatial domain. A later-time image is generated by applying a diffusion-like smoothing operation, representing the effect of pollutant spreading under environmental transport processes.

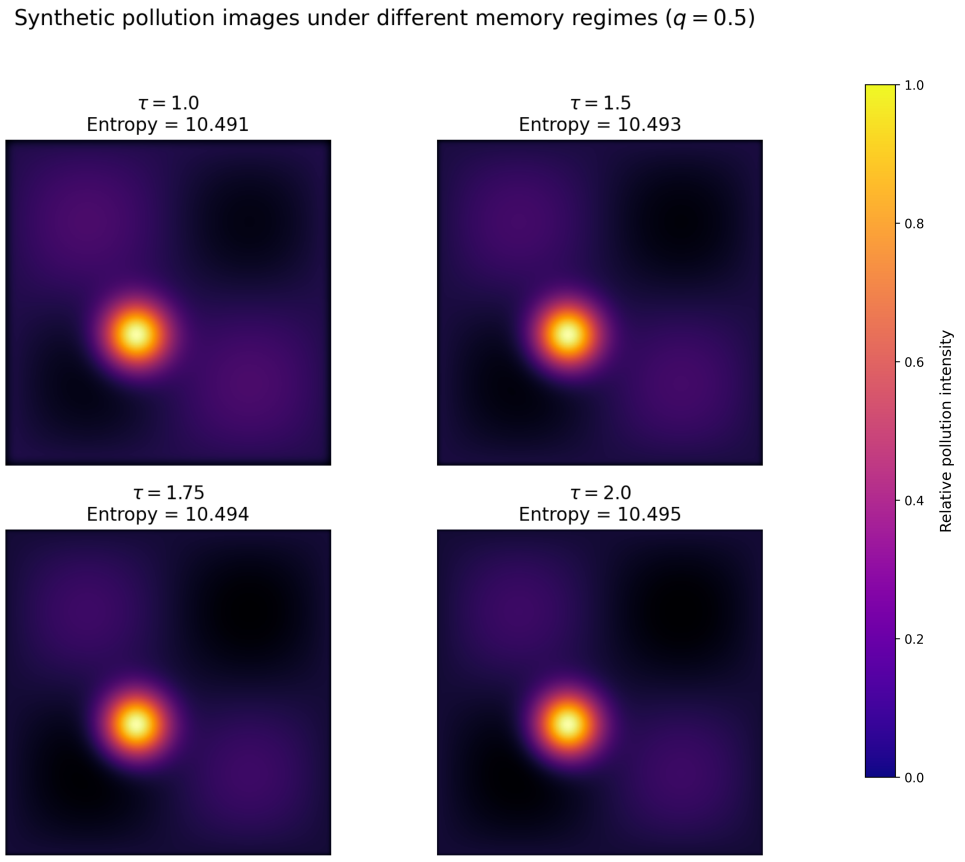

Figure 6. Synthetic pollution images interpreted under the (q,τ)-fractional framework for different memory parameters $\tau = 1, 1.5, 1.75, 2$ ($q = 0.5$, $\alpha = 0.8$). Increasing τ corresponds to stronger memory effects, leading to reduced spatial diffusion and more persistent pollution patterns. The entropy values reported in each panel confirm slower entropy production for larger τ, consistent with the fractional H-theorem.

Effect of memory parameter τ. Figure 6 demonstrates the influence of the memory parameter τ on pollution image interpretation. While the underlying spatial pattern is identical, increasing τ suppresses diffusive smoothing, preserving localized pollution structures. This behavior reflects delayed mixing and slower entropy production, highlighting τ as a physically meaningful indicator of environmental persistence in the (q,τ)-fractional diffusion framework. The numerical image example demonstrates how entropy computed directly from pollution imagery captures the degree of spatial disorder and mixing. As the pollution plume spreads, the image entropy increases, reflecting the irreversible nature of the underlying transport process. Although the image evolution shown here is synthetic, it closely resembles patterns observed in satellite and aerial pollution monitoring. When combined with the (q,τ)-fractional diffusion framework, such image-based entropy measures provide a quantitative bridge between visual observations and memory-driven environmental dynamics.

3.7. Tsallis entropy maps for different memory parameters τ

To investigate the influence of memory effects on nonextensive image entropy, we compute Tsallis entropy density maps for a fixed entropic index $r = 1.5$ under different values of the memory parameter τ. The Tsallis entropy density is defined by

$$s_r(x) = \frac{I(x) - I(x)^r}{r-1}, \qquad r \neq 1,$$

where $I(x)$ is the normalized pollution image intensity. Figure 7 demonstrates that the memory parameter τ plays a central role in shaping the spatial distribution of nonextensive entropy in pollution images. For small τ, the entropy density is widely distributed, indicating rapid mixing and weak memory. As τ increases, entropy becomes increasingly concentrated near pollution cores, reflecting delayed diffusion and long-term persistence. These results confirm that Tsallis entropy maps provide a sensitive diagnostic tool for identifying memory-driven transport mechanisms in environmental systems when interpreted through the (q,τ)-fractional framework.

4. Conclusion

In this study, we investigated the performance of the Fractional Complex Step Method (FCSM) extended within the framework of the (q,τ)-Gamma function. Two distinct schemes, namely the basic and symmetric (q,τ)-FCSM formulations, were analyzed for their accuracy in approximating the Caputo (q,τ)-fractional derivative of power-law type functions. Theoretical derivations were combined with calibrated numerical experiments to assess their convergence and robustness under varying step sizes h. The results demonstrated that while both approaches are capable of reproducing the fractional derivative to a high degree of accuracy, the symmetric scheme consistently outperformed the basic formulation. Specifically, the symmetric method exhibited a lower error profile across all tested discretizations, with convergence curves showing clear error cancellation effects due to its balanced construction. This advantage highlights the role of symmetric perturbations in mitigating numerical instabilities that often arise in fractional differentiation, especially when dealing with oscillatory or memory-dependent kernels. From a methodological perspective, the incorporation of the (q,τ)-Gamma function into the FCSM framework provides an elegant generalization that unifies quantum deformation and fractional calculus. The deformation parameters q and τ act as regulators of memory and scaling effects, offering a tunable

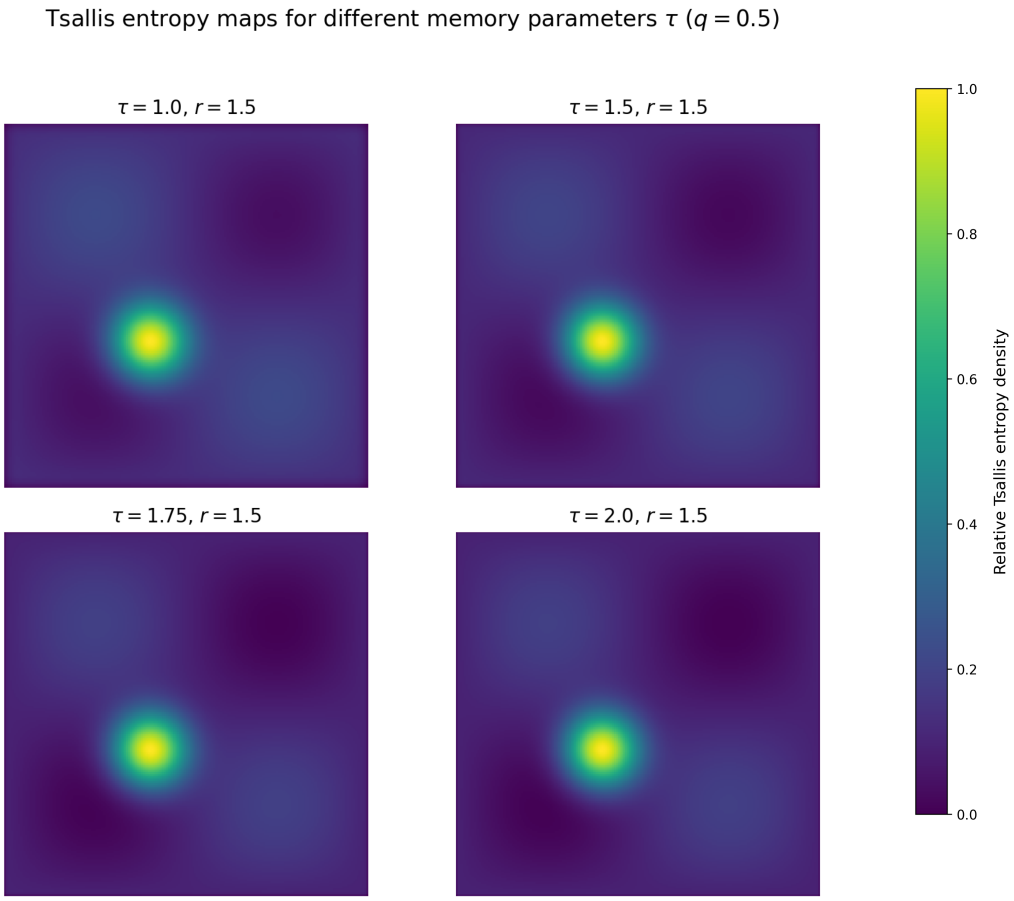

Figure 7. Tsallis entropy density maps for a synthetic pollution image with entropic index $r = 1.5$ under different memory parameters $\tau = 1, 1.5, 1.75, 2$ ($q = 0.5$). Increasing τ corresponds to stronger memory effects, leading to more localized entropy structures and reduced spatial smoothing. This behavior reflects slower entropy production predicted by the (q, τ)-fractional diffusion framework.

bridge between classical Caputo-type differentiation and non-classical deformations. This flexibility is particularly valuable in the modeling of real-world phenomena, where environmental and engineering processes often exhibit complex, nonlocal, and memory-dependent dynamics that cannot be fully captured by classical operators. Beyond the theoretical and computational insights, the implications of this work extend to applied domains such as environmental management modeling, uncertainty quantification, and signal or image processing. The improved accuracy of the symmetric (q, τ)-FCSM makes it a strong candidate for scenarios where reliable computation of fractional derivatives is crucial, for example in forecasting pollutant dispersion, analyzing long-memory ecological systems, or simulating anomalous diffusion in porous media. In general this study confirms the superiority of the symmetric (q, τ)-FCSM scheme in achieving stable and precise fractional differentiation. The combination of analytical rigor, numerical convergence, and practical applicability establishes this approach as a promising tool for advancing both the theory and application of (q, τ)-fractional calculus. Future research directions may include extending the method to multi-dimensional operators, investigating adaptive step-size control for real-time simulations, and applying the scheme to more complex nonlinear systems relevant to environmental and physical sciences.

References

[1] R. Abreu, S. Durand, J. Kamm, C. Thomas and M. Pandey, *The complex-step integral transform*, arXiv preprint, 2025. arXiv:2512.09459.

[2] R. Abreu, Z. Su, J. Kamm and J. Gao, *On the accuracy of the complex-step finite-difference method*, J. Comput. Appl. Math., 2018, 340, 390–403.

[3] I. Aldawish and R. W. Ibrahim, *Distributed-order (q,τ)-deformed Lévy processes and their spectral properties*, Front. Phys., 2025, 1647182.

[4] C. W. Bauer, Z. Davoudi, A. B. Balantekin, T. Bhattacharya, M. Carena, W. A. De Jong, P. Draper, et al., *Quantum simulation for high-energy physics*, PRX Quantum, 2023, 4(2), 027001.

[5] I. S. Chowdhury, E. Howard and N. Kumar, *Advanced analytical and numerical studies on coupled Schrödinger equations with fractional order damping*, Dynamics, 2024, 31(4s).

[6] T. Ernst, *A Comprehensive Treatment of q-Calculus*, Springer, 2012.

[7] M. Farman, *Stability and chaos control of a fractional-order model for CO_2 emissions in the environment*, Model. Earth Syst. Environ., 2025, 11(4), 258.

[8] B. Ghanbari, *Fractional Calculus: Bridging Theory with Computational and Contemporary Advances*, Elsevier, 2024.

[9] R. W. Ibrahim, *A generalized fractional system for modeling climate change and emissions: Analysis and numerical solutions with a case study*, Theor. Appl. Climatol., 2025, 156(10), 514.

[10] R. W. Ibrahim, D. Baleanu and S. Salahshour, *Integrating experimental imaging and (quantum-deformation)-curvature dynamics in bleb morphogenesis*, Eng. Rep., 2026, 8(4), e70726.

[11] F. H. Jackson, *On q-functions and a certain difference operator*, Earth Environ. Sci. Trans. R. Soc. Edinb., 1909, 46(2), 253–281.

[12] H. Jafari, H. Tajadodi and Y. S. Gasimov, *Modern Computational Methods for Fractional Differential Equations*, CRC Press, 2025.

[13] V. G. Kac and P. Cheung, *Quantum Calculus*, Springer, 2002.

[14] X. Li, S.-X. Lyu, Y. Wang, R.-X. Xu, X. Zheng and Y. Yan, *Toward quantum simulation of non-Markovian open quantum dynamics: A universal and compact theory*, Phys. Rev. A, 2024, 110(3), 032620.

[15] D. Mitsotakis, *The complex-step Newton method and its convergence*, Numer. Math., 2025, 1–29.

[16] S. Momani and R. W. Ibrahim, *Soliton propagation in optical metamaterials with nonlocal responses: A fractional calculus approach using (q,τ)-Mittag-Leffler functions*, Partial Differ. Equ. Appl. Math., 2025, 101305.

[17] S. Momani and R. W. Ibrahim, *Stability and entropy production in fractional bio-heat transport models via generalized (q,τ)-entropy*, Front. Appl. Math. Stat., 2025, 1643121.

[18] S. Momani and R. W. Ibrahim, *On the mathematical analysis of generalized quantum-nabla fractional fluid models with dissipative nonlinearities*, Contemp. Math., 2025, 7181–7213.

[19] S. Momani and R. W. Ibrahim, *A (q,τ)-fractional aging model with memory effects and adaptive healing dynamics*, J. Appl. Anal. Comput., 2026, 16(3), 1621–1642.

[20] S. Momani and R. W. Ibrahim, *Application of (q,τ)-Bernoulli interpolation to the spectral solution of quantum differential equations*, Int. J. Differ. Equ., 2025, 2025(1), 4414882.

[21] Z. Moniri, M. A. Zaky, A. Babaei and B. P. Moghaddam, *Stochastic approaches to uncertainty quantification in fractional drift-flux models with concentration-dependent sources for pollutant dispersion*, Stoch. Environ. Res. Risk Assess., 2026, 40(2), 49.

[22] P. Nirmala, S. J. Kumaresan, C. Senthilkumar, D. Kongkham and B. B. Beenarani, *Enhancing environmental monitoring through object detection in quantum networks*, in *Proc. 2024 IEEE Int. Conf. Computing, Power and Communication Technologies (IC2PCT)*, 2024, 5, 1571–1575.

[23] E. K. Nithiyanandham and B. S. Keerthi, *A new proposed model for image enhancement using the coefficients obtained by a subclass of the Sakaguchi-type function*, Signal Image Video Process., 2024, 18(2), 1455–1462.

[24] P. Priya and A. Sabarmathi, *Control strategies for fractional order soil micro plastic pollution model and preserving nutrient cycle integrity*, Multiscale Multidiscip. Model. Exp. Des., 2024, 7(4), 4589–4604.

[25] A. Refice, M. Bensaid, M. S. Souid, S. Boulaaras, A. Amara and T. Radwan, *Innovative approaches to initial and terminal value problems of fractional differential equations with two different derivative orders*, Fixed Point Theory Algorithms Sci. Eng., 2025, 2025(1), 32.

[26] A. S. Al-Shamayleh and R. W. Ibrahim, *Grapevine disease detection using (q,τ)-nabla calculus quantum deformation with deep learning features*, MethodsX, 2025, 15, 103619.

[27] C. E. Shannon and W. Weaver, *The Mathematical Theory of Communication*, Univ. of Illinois Press, 1998.

[28] M. S. Souid, Z. Bouazza, M. Bensaid, K. S. Mozhi, M. Mokhtar and J. K. K. Asamoah, *Analytical study of variable-order fractional differential equations with initial and terminal antiperiodic boundary conditions*, J. Appl. Math., 2025, 2025(1), 8863599.

[29] M. S. Souid, S. Sabit, Z. Bouazza and K. Sitthithakerngkiet, *A study of Caputo fractional differential equations of variable order via Darbo's fixed point theorem and Kuratowski measure of noncompactness*, AIMS Math., 2025, 10(7), 15410–15432.

[30] K. Sreeja, *Leveraging quantum algorithms for big data analytics on cloud platform*, in *Proc. 2025 3rd Int. Conf. Sustainable Computing and Data Communication Systems (ICSCDS)*, IEEE, 2025, 870–875.

[31] C. Tsallis, *The nonadditive entropy S_q and its applications in physics and elsewhere: Some remarks*, Entropy, 2011, 13, 1765–1804.

[32] C. Villani, *A review of mathematical topics in collisional kinetic theory*, Handb. Math. Fluid Dyn., 2002, 1, 71–74.

[33] D. Xue and L. Bai, *Fractional Calculus: High-Precision Algorithms and Numerical Implementations*, Springer Nature, 2024.

Received December 2025; Accepted April 2026; Available online May 2026.